January 2018

Relativistic Multireference Perturbation Theory With Applications To D And F Block Metal Systems

Eric Timian

RELATIVISTIC MULTIREFERENCE PERTURBATION THEORY WITH
APPLICATIONS TO *d* AND *f* BLOCK METAL SYSTEMS

by

Eric Benjamin Timian
Bachelor of Science, University of North Dakota, 2011

A Dissertation
Submitted to the Graduate Faculty

of the

University of North Dakota

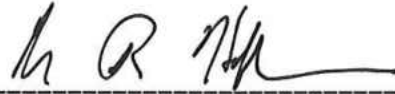in partial fulfillment of the requirements

for the degree of

Doctor of Philosophy

Grand Forks, North Dakota

August
2018

This dissertation, submitted by Eric B. Timian in partial fulfillment of the requirements for the Degree of Doctor of Philosophy from the University of North Dakota, has been read by the Faculty Advisory Committee under whom the work has been done and is hereby approved.
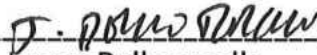
_____
Dr. Mark R. Hoffmann, Chairperson

_____
Dr. Harmon B. Abrahamson

_____
Dr. Kathryn Thomasson

_____
Dr. Jerome Delhommelle

_____
Dr. William Schwalm

This dissertation is being submitted by the appointed advisory committee as having met all of the requirements of the School of Graduate Studies at the University of North Dakota and is hereby approved.

_____
Grant McGimpsey
Dean of the School of Graduate Studies

July 27, 2018
_____
Date

<div align="center">PERMISSION</div>

Title	Relativistic Multireference Perturbation Theory with Applications to d and f block Metal Systems
Department	Chemistry
Degree	Doctor of Philosophy

       In presenting this dissertation in partial fulfillment of the requirements for a degree from the University of North Dakota, I agree that the library of this University shall make it freely available for inspection. I further agree that permission for extensive copying for scholarly purposes may be granted by the professor who supervised my dissertation work or, in his absence, by the Chairperson of the department or the dean of the School of Graduate Studies. It is understood that any copying or publication or other use of this dissertation or part thereof for financial gain shall not be allowed without my written permission. It is also understood that due recognition shall be given to me and to the University of North Dakota in any scholarly use which may be made of any material in my dissertation.

<div align="right">Eric Timian
August 2018</div>

TABLE OF CONTENTS

LIST OF FIGURES

LIST OF TABLES

ACKNOWLEDGEMENTS

I would like to express my sincerest appreciation and gratitude to the members of my advisory Committee for their guidance and support during my graduate career at the University of North Dakota, to the funding agencies that supported my research, to members of my research group for helpful discussions and insight, and to my family and friends for their continued moral support, motivation, and some really fun times.

ABSTRACT

Electronic structure theory programs strive to be as widely applicable as possible. In order to account for effects exhibited by heavier elements, relativistic considerations must be incorporated into these programs. The methods developed in recent years generally succeed in describing the relativistic nature of systems containing heavier elements with reasonable accuracy, but have limited application due to their complexity and computational demand. Highly correlated systems exhibiting significant relativistic effects remain as a challenge to quantum chemical methods.

In this thesis, I present the application of a well-defined relativistic Hamiltonian to a high-level electronic structure theory to generate a relativistic variant of a high-level multireference electronic structure theory capable of obtaining accurate results for highly correlated relativistic systems. This theory applies the exact two-component (X2C) relativistic Hamiltonian and a third-order Douglass-Kroll-Hess (DKH3) transformation for the spin-free and spin-orbit terms, respectively. The spin-orbit integrals are contracted into an effective one-electron Hamiltonian using the atomic mean field (AMFI) approximation, which increases computational efficiency with little loss in accuracy. By applying this scheme to the second-order generalized van Vleck perturbation theory (GVVPT2), which offers appropriate treatment of electron correlation, a theory providing an accurate analysis of chemical systems with strong relativistic effects is obtained.

ix

The method developed in this work is used to explore ground and low-lying excited states of the lanthanide dimer systems Gd_2 and Dy_2. Results from scalar relativistic studies show that GVVPT2 can accurately characterize these systems. The ground electronic states obtained (Gd_2: $^{19}\Sigma_g^-$; Dy_2: $^{11}\Pi_g$) match literature and theoretical results. The spectroscopic data obtained for the ground state of Gd_2 ($R_e = 2.826$ Å; $D_e = 2.48$ eV; $\omega_e = 153.0$ cm^{-1}) are in excellent agreement with literature values ($R_e = 2.877$ Å; $D_0 = 2.1 \pm 0.7$ eV; $\omega_e = 138\text{-}149$ cm^{-1}). Inclusion of spin-orbit coupling in these studies is expected to improve the results to agree with literature values to within chemical accuracy. Future work is planned to extend this method to transition metal trimers.

CHAPTER I

INTRODUCTION

Computational chemistry serves as a cornerstone to modern chemistry research. As new molecules and materials are developed, theoretical calculations on them are necessary in order to gain a more complete understanding. The methods used to perform these calculations must treat the more important effects with sufficient accuracy in order to provide a decent description of the system. While the largest electronic effects in chemical problems are Coulomb and exchange correlation, an accurate description of the electron correlation is essential in order to achieve chemical accuracy (~1 kcal/mol), even though it accounts for only a small amount of the total energy (<1%).[1] When considering molecules and materials containing heavier elements, other physical effects become more pronounced, such as relativity. For example, scalar relativistic effects in gold reduce the energy gap between the 5d and 6s orbitals, which allows the electronic transitions between these orbitals to occur within the visible spectrum, giving it a lustrous and brilliant color. Otherwise, gold would have the same color as silver.[2] For materials exhibiting large relativistic effects, it is as equally important as electron correlation to have an accurate description of these effects.[3] Therefore, more sophisticated methods that go beyond the simple nonrelativistic limit are required in order to gain a full understanding of the system under study. Such methods are in general more sophisticated than their nonrelativistic counterparts and, as a result, have seen less computational development.

1

Scalar-Relativistic Effects

The main relativistic effects present within chemical systems can be categorized as either scalar-relativistic or spin-dependent contributions, of which spin-orbit contributions are most important. Scalar-relativistic effects primarily manifest as changes in orbital sizes due to a relativistic mass increase in the electron. The mass of a 1s electron is represented as[2]

$$m = \gamma m_e = \frac{m_e}{\sqrt{1 - v_{1s}^2/c^2}} \tag{1.1}$$

where the velocity of a 1s electron is equal to the nuclear charge in atomic units ($v_{1s} = Z \, a.u.$) and $c = 137.0359998 \, a.u.$ The Bohr radius is inversely proportional to the electron mass

$$a_0 = \frac{4\pi\varepsilon_0\hbar^2}{m}. \tag{1.2}$$

So, as the atomic number increases to a size such that Z^2 is comparable to c^2, relativity will contract a one-electron atom. This concept can be extended to many-electron atoms by considering the relativistic correction to the orbitals. It has been shown that, for a property a of atomic orbital μ, for inner core as well as outer valence orbitals of a given symmetry type l, j,[4]

$$\delta a_\mu \simeq c_{l,j}^a \left(\frac{Z}{c}\right)^2, \tag{1.3}$$

where Z is the unshielded nuclear charge. Thus, the relativistic correction for heavier atoms is larger than predicted by the hydrogenic model. This direct relativistic effect leads to a predominant stabilization and consequential contraction of the s and p atomic orbitals.

The relativistic change of the inner atomic orbitals induces a change of electronic shielding of the nuclear attraction, which results in a change in the potential energy of the orbitals. Due to the relativistically contracted inner core orbitals, this indirect relativistic effect arises as an energetic destabilization and consequential expansion of the outer core orbitals. The effect becomes most prevalent for orbitals in close proximity of each other, such as for valence orbitals with core shells near their maxima. Relativistically contracted semi-core s and p shells have a similar radial extent but much lower energy than valence d and f orbitals and thus exert a strong indirect effect on the valence shell, whereas the direct relativistic stabilization of the valence d and f orbitals is rather weak. Therefore, relativistic expansion remains predominant for the d and f atomic orbitals.[2–5]

Spin-Orbit Coupling

The other main contribution to relativistic effects is spin-orbit interactions. The basic mechanism of spin-orbit interactions can be interpreted as magnetic induction. More definitively, for an electron moving in a molecular field, spin-orbit coupling (SOC) describes the interaction of the spin of the electron with the magnetic field due to the relative motion of the charges. This interaction can be expressed more explicitly by considering a nonzero electrostatic potential contribution to the Hamiltonian, such is the

3

case for interactions between the electron and a nucleus in an atom. This potential can be represented by $\varphi = V(r)$. The electric field due to V is[6]

$$\boldsymbol{E} = -\boldsymbol{\nabla} V = -\frac{\boldsymbol{r}}{r}\frac{dV}{dr}. \tag{1.4}$$

Since the charges are in relative motion with respect to each other, a magnetic field is induced and experienced by the electron given by

$$\boldsymbol{B} = -\frac{\boldsymbol{v}}{c} \times \boldsymbol{E} \tag{1.5}$$

where $\boldsymbol{v}$ is the velocity of the electron. This magnetic field will interact with the intrinsic magnetic moment of the electron and can be represented in the Hamiltonian as

$$H' = -\boldsymbol{\mu} \cdot \boldsymbol{B} \tag{1.6}$$

Representing the magnetic moment as $\boldsymbol{\mu} = \frac{e\hbar}{mc}\boldsymbol{S}$, where $\boldsymbol{S}$ is the spin operator, and substituting the expression for the magnetic field into the Hamiltonian, the interaction is then re-expressed as

$$
\begin{aligned}
H' &= \frac{e\hbar}{mc}\boldsymbol{S} \cdot \left[\frac{\boldsymbol{v}}{c} \times \boldsymbol{E}\right] \\
&= \frac{e\hbar}{mc}\boldsymbol{S} \cdot \left[\frac{\boldsymbol{p}}{mc} \times \left(\frac{\boldsymbol{r}}{r}\frac{dV}{dr}\right)\right] \\
&= -\frac{e\hbar}{m^2c^2}\frac{1}{r}\frac{dV}{dr}(\boldsymbol{L} \cdot \boldsymbol{S})
\end{aligned}
\tag{1.7}
$$

4

where $\boldsymbol{L} = \boldsymbol{r} \times \boldsymbol{p}$ is the angular momentum. This is defined as the spin-orbit interaction, and must be included in the interaction Hamiltonian. A more formal derivation of the spin-orbit term presented by Desai within the Dirac framework[6] is given in Appendix A.

With the inclusion of spin-orbit interactions, l and s are no longer good quantum numbers (even for a central potential), and only the total angular momentum $\boldsymbol{j} = \boldsymbol{l} + \boldsymbol{s}$ is conserved. Orbitals are then characterized by the quantum numbers j and m_j

$$\hat{\jmath}^2 |j, m_j\rangle = \hbar^2 j(j+1)|j, m_j\rangle \tag{1.8}$$

$$\hat{\jmath}_z |j, m_j\rangle = \hbar m_j |j, m_j\rangle. \tag{1.9}$$

This gives rise to orbital splitting $\left(p \to (p_{1/2}, p_{3/2}), d \to (d_{3/2}, d_{5/2}), etc.\right)$ and, consequently, splitting of molecular energy states. The spin-orbit interaction allows for coupling between otherwise non-interacting states, e.g. states with different multiplicities. New relaxation pathways thus open up for electronically excited states via inter-system crossing, and new reaction channels are permitted.[7–9] Reactions of O(^{3}P) or O$_2$($^3\Sigma_g^-$) with unsaturated hydrocarbons typical in combustion processes proceed through triplet diradical formation, and the closed-shell singlet products can only be formed through inter-system crossing.[10–18] Sensitization processes producing singlet oxygen widely used in photochemistry and biomedical applications are driven by spin-orbit coupling.[19] Phosphorescence, an effect resulting from triplet emission, arises due to spin-orbit coupling, and is essential in organic light-emitting devices.[20]

Relativistic Hamiltonians

While relativistic effects are far less pronounced in lighter elements, they have proven to be phenomena that cannot be neglected in molecules containing heavier elements, such as 5d and 6d transition metals, lanthanides, and actinides.[5,21–34] Not only do relativistic effects provide a contribution to the overall energy that is on the order of electron correlation, but a relativistic description of the system under consideration is required to provide an accurate characterization of its physical and chemical properties, such as the orbital picture, bond lengths, or binding energy.[35] Moreover, relativistic effects, such as NMR coupling constants, are prominent in elements as light as carbon.[36,37] In order to account for these effects nonperturbatively in quantum chemical calculations, the four-dimensional Dirac operator is (usually) applied

$$\gamma^\mu \partial_\mu, \tag{1.10}$$

$$\gamma^\mu = (\gamma^1, \gamma^2, \gamma^3, \gamma^4), \qquad \gamma^4 = \begin{pmatrix} \mathbf{1} & \mathbf{0} \\ \mathbf{0} & -\mathbf{1} \end{pmatrix}, \qquad \gamma^i = \begin{pmatrix} \mathbf{0} & \boldsymbol{\sigma}_i \\ -\boldsymbol{\sigma}_i & \mathbf{0} \end{pmatrix}, \tag{1.11}$$

$$\partial_\mu = \left(\partial_x, \partial_y, \partial_z, \frac{1}{c} \partial_t \right), \tag{1.12}$$

where $\boldsymbol{\sigma}_i$ are the Pauli spin matrices. Application of this operator to the generalized eigenvalue problem gives the four-dimensional Dirac Hamiltonian

$$H = c\boldsymbol{\alpha} \cdot \boldsymbol{p} + \beta m_0 c^2. \tag{1.13}$$

While this yields an accurate description of relativistic effects that includes spin-free and spin-orbit interactions, it necessitates the development of four-component quantum

chemical methods, which are computationally expensive relative to their nonrelativistic counterparts due, for example, to the required evaluation and storage of more two-electron integrals than in the nonrelativistic case.[38,39] Furthermore, solving for the relativistic wavefunction introduces complications, such as taking into account the existence of negative energy (positronic) states which are not present for nonrelativistic treatments of electronic structure.[40] The latter can be overcome through a decoupling scheme which eliminates the small component resulting in two-component theories yielding only electronic solutions, which allows the eigenvalue equation to be expressed in terms of the large component only.[41-51] Additional approximations can be made concerning the omission (or approximation) of individual contributions to the Dirac-Coulomb-Breit (DCB) Hamiltonian. The one of central interest to this dissertation is the contraction of the two-electron spin-orbit operator to an effective one-electron operator.[52] Approximations to the DCB operator can significantly reduce computational cost while still capturing spin-orbit interactions for chemical systems for which the approximation is valid.

Several two-component approaches have been developed to approximate the four-dimensional Dirac Hamiltonian. The Douglas-Kroll-Hess (DKH) approach,[42,44,45] which starts with a Foldy-Wouthuysen (FW) transformation,[41] aims to block-diagonalize the Hamiltonian through a series of unitary transformations. Since the transformations have regular forms for higher-order terms, it has been widely used. The Barysz-Sadlej-Snijders (BSS) approach[47] perturbatively expands a two-component Hamiltonian and then follows

7

a two-step block-diagonalization, the first transformation generating the spin-free part of the Hamiltonian, and the subsequent transformation generating the spin-dependent part. This block-diagonalization can, however, be achieved in one-step following the exact two-component (X2C) approach.[51] Alternatively, perturbative expansions, called regular approximations (RA), to the Hamiltonian may also be considered. Different levels of the perturbative truncations of the operator give rise to the different orders of the RA, such as zeroth-order (ZORA), first-order (FORA), etc.[43,46] This dissertation is focused on approximations in the X2C framework.

There have been many efforts to incorporate SOC into methods of electronic structure theory (CI, CC, EOM-CC, MRCC, DFT, CASSCF, CASPT2, MRCI)[53–65] applying a number of different two- or four-component approaches. A study by Liu et al.[66] surveyed the application of various relativistic Hamiltonians to systems exhibiting large relativistic effects. One of the results of that study showed that an X2C treatment of the spin-free terms and a third-order DKH (DKH3) –like treatment of the spin-orbit terms is most practical. Implementing this relativistic Hamiltonian into electronic structure theory methods allows a much larger variety of chemical systems to be studied with reasonable accuracy.

Symmetry in Relativistic Systems

For chemical systems exhibiting relativistic behavior, fundamental characteristics differ significantly from a nonrelativistic representation. Therefore, the symmetry of these

systems must also be reevaluated. While the orbital and spin angular momentum l and s are conserved in a nonrelativistic framework, the total angular momentum $j = l + s$ is the conserved quantity in relativistic systems, yielding either integer (boson) or half-integer (fermion) values. Consequently, the symmetry operation of a rotation through an angle of 2π for a fermionic state returns an inversion of the original state. Thus, the number of symmetry elements for a relativistic system is doubled, and the symmetry group representing the system extends to a double group. Exploitation of symmetry of a chemical system reduces computational cost, so incorporating double group symmetry into electronic structure theories for relativistic systems is sensible. A more detailed discussion of double group symmetry is given in Chapter 2.

Single Molecule Magnets

Materials, whose properties depend strongly on chemical structure, have become of greater and greater interest within the chemistry community in recent years. One of these types of materials is single molecule magnets (SMMs). These materials generally contain a few heavy atoms at their core, commonly consisting of d or f block elements. Since elements of the 5th period and below are strongly affected by relativity, high-level relativistic electronic structure calculations, at least on the isolated cores, are necessary in order to understand their properties. The research presented in this work focuses on lanthanide dimers.

In its ground state, the gadolinium atom displays the highest spin multiplicity of any atom, with an electronic configuration of $[Xe]4f^7 5d^1 6s^2$, resulting in a ground state with atomic symbol of $^9D_2$.[67] Consequently, Gd-containing molecules also exhibit high spin multiplicities, generating interest in, for example, pharmaceutical industries for use as magnetic resonance imaging (MRI) signal enhancers and radiation sensitizers for cancer radiation therapy.[68] As a dimer, the Gd_2 molecule has a ground state electronic configuration of $(4f^7)(4f^7)6s\sigma_g^2 6s\sigma_u^1 5d\sigma_g^1 5d\pi_u^2$. Electron spin resonance (ESR) spectroscopy has revealed that the spectral lines of Gd_2 are best fitted to an $S = 9$ Hamiltonian,[69] indicating that there are 18 unpaired electrons that are ferromagnetically coupled, including the 14 inner $4f$ electrons. This results in a $^{19}\Sigma_g^-$ ground electronic state for the Gd_2 molecule. When considering the dissociation of Gd_2 into separate ground state atoms, a correlation diagram shows that there are four $6s$ electrons and two $5d$ electrons at the dissociation limit. Therefore, Gd_2 will experience an avoided crossing upon dissociation from the ground state. This implies the existence of numerous low-lying excited states which can also be deduced from the atomic energy levels, and, since atomic states with different $5d$ and/or $4f$ occupation may mix in the molecules, careful treatment of electron correlation must be applied.

There have been few previous experimental or theoretical studies of Gd_2. Theoretical calculations for Gd_2 have mainly been published by Dolg and co-workers using a variety of methods. In 1992, Dolg and co-workers performed configuration interaction

(CI) and energy density functional theory (DFT) calculations using scalar-relativistic energy-adjusted *ab initio* pseudopotentials.[70] In that study, the $4f^7$ subshells were treated as part of the core. Their results indicated that the valence substate of the ground electronic state was $^5\Sigma_u$. The atomlike $4f^7$ subshells were expected to be coupled to an ^8S state, meaning that, overall, Gd_2 consists of 18 total unpaired electrons. The obtained spectroscopic data (R_e = 3.015 Å, D_e = 0.98 eV), are in disagreement with later experimental data. The same authors improved upon their earlier results in a 2000 study using configuration interaction including single and double excitations (CISD) and the averaged coupled-pair functional approach (ACPF), and explicitly correlating the 4f orbitals.[71] The results obtained in this study produced a $^{19}\Sigma_u$ ground state with spectroscopic data (R_e = 3.006 Å, ω_e = 117 cm^{-1}, D_e = 1.41 eV) that is in closer agreement with experimental results. Perhaps the best theoretical results obtained for Gd_2 were by the same author in 2003.[72] In that study, relativistic energy-consistent small-core pseudopotentials were applied to the core $1s$-$3d$ shells, while atomic natural orbital (ANO) valence basis sets were used to span the valence shells. Calculations were performed at the coupled cluster level of theory with single, double, and perturbative triple excitations (CCSD(T)). The results from that study showed a $^{19}\Sigma_g^-$ ground electronic state with spectroscopic data (R_e = 2.877 ± 0.020 Å, D_e = 1.60 ± 0.18 eV, ω_e = 149 ± 2 cm^{-1}) in better agreement with experimental data. Due to the large number of low-lying excited states and complexity of the electron correlation, it is clear that a multireference treatment of Gd_2

11

would be highly desired. However, currently available theoretical results have only used single-reference methods, and no full potential energy curves have been generated for this system.

Numerous studies have been conducted involving SMMs containing dysprosium cores. Two underlying conditions for SMM behavior (i.e., doubly-degenerate ground states with high m_j values and large separation between ground and excited states)[73] are easily achieved for Dy-based compounds, which make them favorable targets for use in magnetic applications, such as magnetic resonance imaging (MRI) and SMMs.[74] Furthermore, the SMM behavior of Dy_2 systems can be tuned effectively by the dipolar interactions and exchange coupling, giving polynuclear Dy-based SMMs advantages over their mononuclear counterparts.[75] The dysprosium atoms within these SMM cores commonly exist as trivalent ions and usually are bridged by some other species. Given that the properties of a directly bonded Dy_2 species have not yet been investigated, either experimentally or theoretically, this dissertation addresses this hole in understanding.

The dysprosium atom has a ground electronic configuration of $[Xe]4f^{10}6s^2$, and results in a ground state with atomic term symbol of $^5I_8$ ($l = 6$). The first excited state with odd parity corresponds to promoting an electron from the f manifold, giving it an electronic configuration of $[Xe]4f^95d6s^2$ with a term symbol of $^7H_8$ ($l = 5$) lying 0.94 eV above the ground state, while the first excited state with even parity corresponds to promoting an electron from the s manifold, giving it an electronic configuration of $[Xe]4f^{10}5d6s$ with a

term symbol of $^3K_9$ ($l = 8$) lying 2.17 eV above the ground state.[67] Dimeric species of dysprosium yield a ground state molecule with a multiplicity of 11, and excited states with multiplicities of 9 (even) and 13 (odd) in addition to 11. The large number of open subshells, especially those arising from more than one subshell, as well as the large angular momentum values, make it an interesting but difficult target for computational study. As stated above, no previous theoretical studies of Dy_2 are in the literature.

For the materials considered for magnetic applications, it is not uncommon for these systems to contain metallic clusters of more than two atoms, providing motivation for studies into these clusters. A logical first step toward these clusters is to consider the scandium trimer, Sc_3, which also proves to be a remarkable and challenging compound to study. The scandium atom contains only one unpaired electron in its valence shell. Therefore, if the three lone electrons remain localized to their respective atomic sites, Sc_3 will have an electronic state subject to spin frustration. Such systems can be extended into lattices with interesting magnetic properties, and also exhibit unusual behavior at low temperatures.

In summary, I describe advances necessary for a relativistic variant of GVVPT2, which provides appropriate treatment of electron correlation, that is both accurate and efficient. The methods used to develop the relativistic theory are reviewed in Chapter 2. Implementation of the sf-X2C+so-DKH3 Hamiltonian capable of describing scalar and spin-orbit relativistic effects, as well as an effective one-electron spin-orbit Hamiltonian

into the GVVPT2 electronic structure theory is described in Chapter 3. Studies of the gadolinium dimer, the dysprosium dimer, and the scandium trimer, using new programs that incorporate relativistic effects, are presented in Chapters 4, 5, and 6, respectively.

CHAPTER II

METHODS

Efforts to extend the GVVPT2 method to include relativistic effects have been in progress in recent years. W. Jiang determined nonvanishing one-electron spin-orbit Hamiltonian matrix elements in cartesian coordinates for CI and GVVPT2 theories.[76] The integrals discussed in that work have since been implemented within the UNDMOL electronic structure package, and used by P. Tamukong in a scalar-relativistic GVVPT2 study that successfully characterized transition metal dimers.[77] The work presented in this dissertation extends on the current scalar-relativistic implementation within UNDMOL to include two-electron spin-orbit coupling effects. Here, I will start with a review of the different methods supplementary to these developments.

The Exact Two-Component Approach

The formulation of the X2C approach presented here follows that of Liu and co-workers.[78] First, consider the Dirac equation for an electron in the presence of an external potential V

$$h^D \psi = E\psi, \tag{2.1}$$

$$h^D = \begin{pmatrix} V & c\vec{\sigma} \cdot \vec{p} \\ c\vec{\sigma} \cdot \vec{p} & V - 2c^2 \end{pmatrix}, \tag{2.2}$$

$$\psi = \begin{pmatrix} \psi^L \\ \psi^S \end{pmatrix} \tag{2.3}$$

where the rest mass energy mc^2 of the electron has been subtracted. The wavefunction is a four-component vector consisting of two bispinors, the large component ψ^L, which corresponds to electronic states, and the small component ψ^S, which corresponds to the positronic state. The Dirac Hamiltonian h^D could be separated into spin-free and spin-dependent parts simply by partitioning h^D into a diagonal and off-diagonal term. However, transforming the Dirac equation according to some metric to form an equivalent modified Dirac equation and then performing the partition is more beneficial. The transformation is chosen such that the small-component spinor ψ^S is expressed in terms of a pseudo-large spinor φ^L while leaving the large-component spinor ψ^L unchanged. This allows ψ^L and φ^L to be expanded in the same basis set. Thus, the transformation can be written as

$$\tilde{T} = \begin{pmatrix} 1 & 0 \\ 0 & R\dfrac{\vec{\sigma} \cdot \vec{p}}{2c} \end{pmatrix}, \qquad \psi^S = R\dfrac{\vec{\sigma} \cdot \vec{p}}{2c}\varphi^L, \tag{2.4}$$

where R is independent of spin. The modified Dirac equation can then be expressed as

$$h^M \psi^M = EM\psi^M, \tag{2.5}$$

with

$$h^M = \tilde{T}^\dagger h^D \tilde{T} = \begin{pmatrix} V & \dfrac{1}{2}(\vec{\sigma} \cdot \vec{p})R(\vec{\sigma} \cdot \vec{p}) \\ \dfrac{1}{2}(\vec{\sigma} \cdot \vec{p})R^\dagger(\vec{\sigma} \cdot \vec{p}) & \dfrac{\alpha^2}{4}(\vec{\sigma} \cdot \vec{p})R^\dagger(V - 2c^2)R(\vec{\sigma} \cdot \vec{p}) \end{pmatrix}, \tag{2.6}$$

$$M = \tilde{T}^\dagger \tilde{T} = \begin{pmatrix} 1 & 0 \\ 0 & \dfrac{\alpha^2}{4}(\vec{\sigma} \cdot \vec{p})R^\dagger R(\vec{\sigma} \cdot \vec{p}) \end{pmatrix}, \tag{2.7}$$

16

$$\psi^M = \tilde{T}^{-1}\psi = \begin{pmatrix} \psi^L \\ \varphi^L \end{pmatrix}. \tag{2.8}$$

Here, $R = 1$ is chosen, which corresponds to the original modified Dirac equation introduced by Kutzelnigg and later studied by Dyall. The transformed Hamiltonian and metric can then be reduced to

$$h^M = \begin{pmatrix} V & T \\ T & \dfrac{\alpha^2}{4}W - T \end{pmatrix}, \tag{2.9}$$

$$T = \frac{\vec{p}^2}{2}, \qquad W = (\vec{\sigma}\cdot\vec{p})V(\vec{\sigma}\cdot\vec{p}), \tag{2.10}$$

$$M = \begin{pmatrix} 1 & 0 \\ 0 & \dfrac{\alpha^2}{2}T \end{pmatrix}. \tag{2.11}$$

The spin dependence now only appears in W within h^M, and so spin separation is easily achieved by using the Dirac identity

$$h^M = h_{sf}^M + h_{sd}^M, \tag{2.12}$$

$$h_{sf}^M = \begin{pmatrix} V & T \\ T & \dfrac{\alpha^2}{4}W_{sf} - T \end{pmatrix}, \qquad h_{sd}^M = \begin{pmatrix} 0 & 0 \\ 0 & \dfrac{\alpha^2}{4}W_{sd} \end{pmatrix}, \tag{2.13}$$

where

$$W_{sf} = \vec{p}\cdot V\vec{p}, \tag{2.14}$$

$$W_{sd} = i\vec{\sigma}\cdot(\vec{p}V \times \vec{p})$$

$$= \vec{\sigma}\cdot[(\nabla V) \times \vec{p}]. \tag{2.15}$$

For the nuclear attraction $V = -\dfrac{Z}{r}$, $(\nabla V) = \dfrac{Z\vec{r}}{r^3}$, so

17

$$W_{sd} = \frac{Z}{r^3} \vec{\sigma} \cdot (\vec{r} \times \vec{p})$$

$$= \frac{Z}{r^3} \vec{\sigma} \cdot \vec{l}$$

$$= \frac{2Z}{r^3} \vec{s} \cdot \vec{l}. \tag{2.16}$$

This shows that W_{sd} is directly connected to spin-orbit coupling.

The previous derivation was carried out within the restricted kinetic balance (RKB).[79] Under the RKB, the large and small components are expanded in the basis sets $\{g_\mu\}$ and $\{f_\mu\}$, respectively

$$\psi_i^L = \sum_{\mu=1}^{2N^L} g_\mu A_{\mu i}, \qquad \psi_i^S = \sum_{\mu=1}^{2N^L} f_\mu B_{\mu i}. \tag{2.17}$$

A relation is then imposed directly between the individual basis functions

$$f_\mu = \frac{\vec{\sigma} \cdot \vec{p}}{2c} g_\mu, \tag{2.18}$$

allowing for evaluation of relativistic properties following the above derivation while avoiding variational collapse.

Although these derivations were carried out at the operator level, it can readily be verified that the matrix representation of h^M in the basis $\{g_\mu\} \cup \{g_\mu\}$ and that of h^D in the basis $\{g_\mu\} \cup \{f_\mu\}$ are the same. The corresponding matrix equations can be expressed as

$$\mathbf{h}^D \mathbf{C} = \mathbf{MC}E, \tag{2.19}$$

$$\mathbf{h}^D = \begin{pmatrix} \mathbf{V} & \mathbf{T} \\ \mathbf{T} & \dfrac{\alpha^2}{4}\mathbf{W} - \mathbf{T} \end{pmatrix} = \mathbf{h}^D_{sf} + \mathbf{h}^D_{sd}, \tag{2.20}$$

$$\mathbf{h}^D_{sf} = \begin{pmatrix} \mathbf{V} & \mathbf{T} \\ \mathbf{T} & \dfrac{\alpha^2}{4}\mathbf{W}_{sf} - \mathbf{T} \end{pmatrix}, \qquad \mathbf{h}^D_{sd} = \begin{pmatrix} \mathbf{0} & \mathbf{0} \\ \mathbf{0} & \dfrac{\alpha^2}{4}\mathbf{W}_{sd} \end{pmatrix}, \tag{2.21}$$

$$\mathbf{M} = \begin{pmatrix} \mathbf{S} & \mathbf{0} \\ \mathbf{0} & \dfrac{\alpha^2}{2}\mathbf{T} \end{pmatrix}, \qquad \mathbf{C} = \begin{pmatrix} \mathbf{A} \\ \mathbf{B} \end{pmatrix}. \tag{2.22}$$

Now that spin separation has been achieved, the large and small components can be decoupled and the small component eliminated. For simplicity, the generic generalized eigenvalue problem is considered

$$\mathbf{hC} = \mathbf{MC}E, \tag{2.23}$$

with

$$\mathbf{h} = \begin{pmatrix} \mathbf{h}_{11} & \mathbf{h}_{12} \\ \mathbf{h}_{21} & \mathbf{h}_{22} \end{pmatrix} = \mathbf{h}^\dagger, \tag{2.24}$$

$$\mathbf{M} = \begin{pmatrix} \mathbf{S}_{11} & \mathbf{0} \\ \mathbf{0} & \mathbf{S}_{22} \end{pmatrix} = \mathbf{M}^\dagger, \tag{2.25}$$

and $\mathbf{C}$ remains as defined previously. A decoupling matrix $\mathbf{X}$ is now introduced by imposing the key relation between the small and large component coefficients

$$\mathbf{B} = \mathbf{XA} \tag{2.26}$$

or

$$\mathbf{X} = \mathbf{BA}^{-1}$$

$$= (\mathbf{BA}^\dagger)(\mathbf{AA}^\dagger)^{-1}. \tag{2.27}$$

19

This leads to a normalized elimination of the small component

$$\mathbf{L}_+^{NESC}\mathbf{A} = \tilde{\mathbf{S}}_+\mathbf{A}E, \tag{2.28}$$

$$\mathbf{L}_+^{NESC} = \mathbf{h}_{11} + \mathbf{h}_{12}\mathbf{X} + \mathbf{X}^\dagger\mathbf{h}_{21} + \mathbf{X}^\dagger\mathbf{h}_{22}\mathbf{X}, \tag{2.29}$$

$$\tilde{\mathbf{S}}_+ = \mathbf{S}_{11} + \mathbf{X}^\dagger\mathbf{S}_{22}\mathbf{X}. \tag{2.30}$$

Currently, this problem remains in the Dirac picture. A unitary transformation must be applied in order to change into the Schrödinger picture

$$\mathbf{U} = \mathbf{U}_N\mathbf{U}_D, \tag{2.31}$$

$$\mathbf{U}_N = \begin{pmatrix} \mathbf{R}_+^\dagger & \mathbf{0} \\ \mathbf{0} & \mathbf{R}_-^\dagger \end{pmatrix}, \tag{2.32}$$

$$\mathbf{U}_D = \begin{pmatrix} \mathbf{I} & \mathbf{X}^\dagger \\ \tilde{\mathbf{X}}^\dagger & \mathbf{I} \end{pmatrix}, \tag{2.33}$$

where

$$\mathbf{R}_+ = \left(\mathbf{S}_{11}^{-1}\tilde{\mathbf{S}}_+\right)^{-\frac{1}{2}} = \mathbf{S}_{11}^{-\frac{1}{2}}\left(\mathbf{S}_{11}^{-\frac{1}{2}}\tilde{\mathbf{S}}_+\mathbf{S}_{11}^{-\frac{1}{2}}\right)^{-\frac{1}{2}}\mathbf{S}_{11}^{\frac{1}{2}}, \tag{2.34}$$

$$\mathbf{R}_- = \left(\mathbf{S}_{22}^{-1}\tilde{\mathbf{S}}_-\right)^{-\frac{1}{2}} = \mathbf{S}_{22}^{-\frac{1}{2}}\left(\mathbf{S}_{22}^{-\frac{1}{2}}\tilde{\mathbf{S}}_-\mathbf{S}_{22}^{-\frac{1}{2}}\right)^{-\frac{1}{2}}\mathbf{S}_{22}^{\frac{1}{2}}, \tag{2.35}$$

$$\tilde{\mathbf{S}}_- = \mathbf{S}_{22} + \tilde{\mathbf{X}}^\dagger\mathbf{S}_{11}\tilde{\mathbf{X}}, \tag{2.36}$$

$$\tilde{\mathbf{X}} = -\mathbf{S}_{11}^{-1}\mathbf{X}^\dagger\mathbf{S}_{22}. \tag{2.37}$$

Constructing the unitary transformation matrix in this way allows the Hamiltonian to be decoupled (achieved by $\mathbf{U}_D$) and renormalized (achieved by $\mathbf{U}_N$). Therefore, applying this transformation to the Hamiltonian and the metric gives

$$\mathbf{UhU}^{\dagger} = \begin{pmatrix} \mathbf{h}_+ & \mathbf{0} \\ \mathbf{0} & \mathbf{h}_- \end{pmatrix}, \qquad \mathbf{UMU}^{\dagger} = \begin{pmatrix} \mathbf{S}_+ & \mathbf{0} \\ \mathbf{0} & \mathbf{S}_- \end{pmatrix}. \tag{2.38}$$

Substituting these relations into the matrix Dirac equation yields

$$\mathbf{UhU}^{\dagger}(\mathbf{U}^{\dagger})^{-1}\mathbf{C} = \mathbf{UMU}^{\dagger}(\mathbf{U}^{\dagger})^{-1}\mathbf{C}E, \tag{2.39}$$

which gives

$$\begin{pmatrix} \mathbf{h}_+ & \mathbf{0} \\ \mathbf{0} & \mathbf{h}_- \end{pmatrix}\begin{pmatrix} \mathbf{C}_+ & \mathbf{0} \\ \mathbf{0} & \mathbf{C}_- \end{pmatrix} = \begin{pmatrix} \mathbf{S}_+ & \mathbf{0} \\ \mathbf{0} & \mathbf{S}_- \end{pmatrix}\begin{pmatrix} \mathbf{C}_+ & \mathbf{0} \\ \mathbf{0} & \mathbf{C}_- \end{pmatrix}\begin{pmatrix} E_+ & \mathbf{0} \\ \mathbf{0} & E_- \end{pmatrix}. \tag{2.40}$$

Choosing the upper-left block of this equation yields an expression for the electrons only

$$\mathbf{h}_+\mathbf{C}_+ = \mathbf{S}_{11}\mathbf{C}_+ E_+, \tag{2.41}$$

$$\mathbf{h}_+ = \mathbf{R}_+^{\dagger}\mathbf{L}_+^{NESC}\mathbf{R}_+, \tag{2.42}$$

$$\mathbf{C}_+ = \mathbf{R}_+^{-1}\mathbf{A}_+. \tag{2.43}$$

Following this scheme, the small component has been removed from the equation, thus producing a two-component theory (in this case, X2C) within a no-pairs approximation from the initial four-component problem. This greatly reduces computational overhead by eliminating the evaluation of the negative energy (positronic) states without sacrificing accuracy of the desired positive energy (electronic) states.

The Douglas-Kroll-Hess Approach

Another technique developed to decouple the Dirac Hamiltonian is the DKH method.[42,44,45] This approach aims to block-diagonalize the Hamiltonian step-wise through a series of unitary transformations[78]

$$\mathbf{h}_{bd}^{DKH} = \cdots \mathbf{U}_3 \mathbf{U}_2 \mathbf{U}_1 \mathbf{U}_0 \mathbf{h}^D \mathbf{U}_0^\dagger \mathbf{U}_1^\dagger \mathbf{U}_2^\dagger \mathbf{U}_3^\dagger \cdots. \tag{2.44}$$

The first transformation in this scheme is defined to be the free-particle FW (fpFW) transformation[41]

$$\mathbf{h}_1 = \mathbf{U}_0 \mathbf{h}^D \mathbf{U}_0^\dagger \tag{2.45}$$

$$= \boldsymbol{\mathcal{E}}_0 + \boldsymbol{\mathcal{E}}_1 + \boldsymbol{\mathcal{O}}_1. \tag{2.46}$$

The unitary operator $\mathbf{U}_0$ in this equation can be expressed as[80]

$$\mathbf{U}_0 = \begin{pmatrix} \mathcal{P} & \mathcal{P}Q \\ -\mathcal{P}Q & \mathcal{P} \end{pmatrix}, \tag{2.47}$$

where $\mathcal{P}$ and Q are kinematical operators defined by

$$\mathcal{P} = \left(\frac{\varepsilon_0 + c^2}{2\varepsilon_0} \right)^{\frac{1}{2}}, \tag{2.48}$$

$$Q = \frac{c\vec{\sigma} \cdot \vec{p}}{\varepsilon_0 + c^2}, \tag{2.49}$$

with

$$\varepsilon_0 = (p^2 c^2 + c^4)^{\frac{1}{2}}. \tag{2.50}$$

The resultant Hamiltonian $\mathbf{h}_1$ in equation (2.45) is identified as the fpFW Hamiltonian, which is also referred to as the no-pair Hamiltonian. The terms $\boldsymbol{\mathcal{E}}_0$, $\boldsymbol{\mathcal{E}}_1$, and $\boldsymbol{\mathcal{O}}_1$ are given by

$$\boldsymbol{\mathcal{E}}_0 = \begin{pmatrix} \varepsilon_0 & 0 \\ 0 & -\varepsilon_0 \end{pmatrix}, \tag{2.51}$$

22

$$\mathcal{E}_1 = \begin{pmatrix} \varepsilon_1 & 0 \\ 0 & \varepsilon_1 \end{pmatrix}, \tag{2.52}$$

$$\mathcal{O}_1 = \begin{pmatrix} 0 & o_1 \\ -o_1 & 0 \end{pmatrix}, \tag{2.53}$$

where

$$\varepsilon_1 = \mathcal{P}V\mathcal{P} + \mathcal{P}QVQ\mathcal{P}, \tag{2.54}$$

$$o_1 = \mathcal{P}QV\mathcal{P} - \mathcal{P}VQ\mathcal{P}. \tag{2.55}$$

The unitary matrices $\mathbf{U}_n$ in equation (2.44) are chosen such that the off-diagonal terms are successively diminished as each transformation is applied. At each step, even (block-diagonal) terms, denoted as $\mathcal{E}$, and odd (off-diagonal) terms, denoted as $\mathcal{O}$, are produced that form the Hamiltonian. If this process is carried out to infinite order, complete decoupling of the Hamiltonian is achieved and a truly block-diagonal form (all odd terms vanish) is obtained[81]

$$\mathbf{h}_{bd}^{DKH} = \sum_{k=0}^{\infty} \mathcal{E}_k$$

$$= \sum_{k=0}^{\infty} \begin{pmatrix} \mathcal{E}_{k+} & 0 \\ 0 & \mathcal{E}_{k-} \end{pmatrix}$$

$$= \sum_{k=0}^{\infty} \begin{pmatrix} \mathcal{E}_{k+}^{sf} + \mathcal{E}_{k+}^{sd} & 0 \\ 0 & \mathcal{E}_{k-}^{sf} + \mathcal{E}_{k-}^{sd} \end{pmatrix}. \tag{2.56}$$

Performing the block-diagonalization this way supplants a well-defined two-component formalism that consist of matrices bounded below so that variational collapse is avoided.

Since carrying this out to infinite order is not practical, the series is truncated at a pre-defined order, giving rise to the DKHn ($n = 1, 2, ...$) schemes, where n is the index of the last unitary transformation considered. This leads to a partially transformed Hamiltonian

$$\mathbf{h}_{pt} = \sum_{k=0}^{n} \mathcal{E}_k + \sum_{k=n+1}^{\infty} \mathcal{E}_k \tag{2.57}$$

$$= \mathbf{h}_{bd}^{DKHn} + \mathcal{O}(V^n). \tag{2.58}$$

Each unitary matrix $\mathbf{U}_n$ is parameterized in terms of an anti-hermitian operator A_n as a series expansion in A_n given by

$$\mathbf{U}_n = \sum_{i=0}^{\infty} a_{n,i} A_n^i = \mathbf{1} + \sum_{i=1}^{\infty} a_{n,i} A_n^i. \tag{2.59}$$

The zeroth-order term in this series expansion is defined to be the identity operator to ensure that all $\mathcal{E}_k$ of lower order remain unchanged by subsequent transformations. Unitarity of $\mathbf{U}_n$ is governed by the set of expansion coefficients $\{a_{n,i}\}$, which can be optimized in order to (generally) fulfill this condition for a given truncation of the series expansion.

The Atomic Mean Field Approximation

Although two-component methods save a considerable amount of overhead generated from computing negative energy solutions, they are still quite computationally demanding due to the integrals involved in evaluating spin-orbit coupling, i.e., the two-

24

electron spin-orbit integrals. While one can neglect the spin-orbit coupling and instead perform scalar relativistic calculations, which is a fine approximation for lighter elements and singlet ground states isolated from the rest of the spectrum, these effects cannot be ignored for heavier atoms, where spin-dependent relativistic effects provide a significant contribution to the overall energy and characteristics of the system. In order to reduce computational cost while preserving the spin-orbit coupling effects, an approximation must be made to the spin-orbit Hamiltonian.

One of the more useful approximations that can be made is to consider a mean-field. In general, a mean-field approximation is defined by any set of occupation numbers by means of a corresponding Fock operator matrix element. By applying an atomic mean-field to the integrals, the two-electron spin-orbit operator can be approximated as an effective one-electron operator by contracting the two-electron spin-orbit integrals against the one-particle density matrix.[52] The approximate spin-orbit operator is defined by

$$H_{ij}^{AMFI} = \langle i|H^{SO}(1)|j\rangle$$

$$+ \frac{1}{2}\sum_{k} n_k \{\langle ik|H^{SO}(1,2)|jk\rangle - \langle ik|H^{SO}(1,2)|kj\rangle - \langle ki|H^{SO}(1,2)|jk\rangle\} \quad (2.60)$$

where the set $\{n_k\}$ represents the values of the one-particle density matrix. This approximation is applicable to virtually any choice of $H^{SO}(1,2)$.

Generalized van Vleck Second-Order Perturbation Theory

The mathematical foundation of the multireference generalized van Vleck second-order perturbation theory (GVVPT2) stems from self-consistent quasidegenerate perturbation theory (SC-QDPT),[82] where the total Hilbert Space (L) is partitioned into a model (L_M) and external (L_Q) space ($L = L_M \oplus L_Q$). The overall Hamiltonian is partitioned in the same manner. In order to avoid problems with quasidegeneracy and intruder states, the model space is further partitioned into a primary (L_P) and secondary (L_S) space ($L_M = L_P \circ L_S$). This partitioning scheme is illustrated in Figure 2.1.
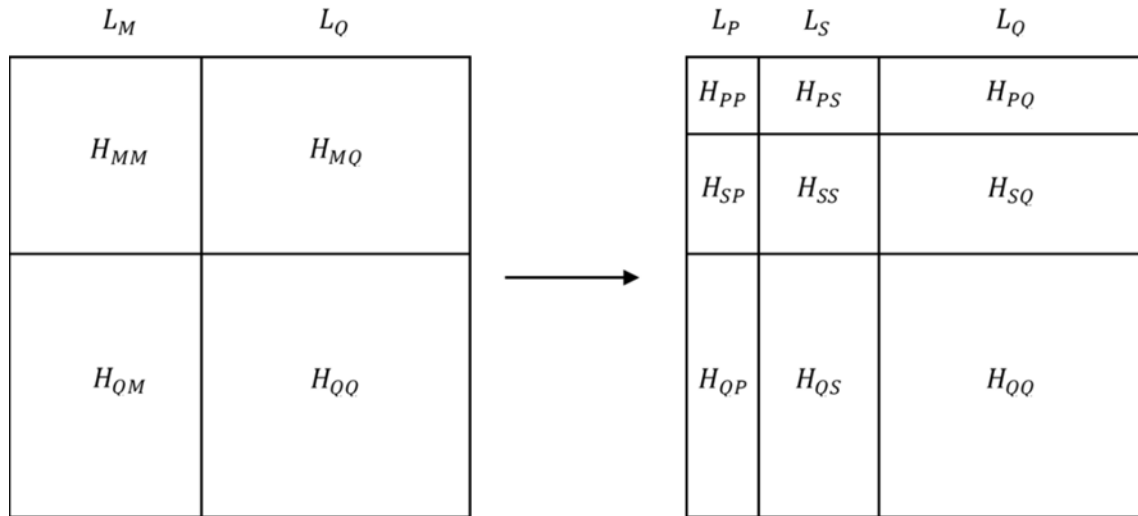
Figure 2.1. Partitioning of the Hamiltonian within SC-QDPT.

In SC-QDPT, the block-diagonal part of the Hamiltonian is then defined as the unperturbed Hamiltonian (H_0), whereas the off-diagonal blocks are treated as a perturbation (V)[83]

$$H_0 = PHP + QHQ = H_{PP} + H_{QQ}, \qquad V = PHQ + QHP$$

$$= H_{PQ} + H_{QP}.$$

(2.61)

An effective Hamiltonian matrix is then formed with four matrix blocks defined as

$$\mathbf{H}_{PP}^{eff} = \mathbf{H}_{PP} + \frac{1}{2}\big(\mathbf{H}_{PQ}\mathbf{X}_{QP} + \mathbf{X}_{QP}^{\dagger}\mathbf{H}_{QP}\big),$$

(2.62)

$$\mathbf{H}_{SP}^{eff} = \mathbf{H}_{SQ}\mathbf{X}_{QP},$$

(2.63)

$$\mathbf{H}_{SS}^{eff} = \mathbf{H}_{SS}.$$

(2.64)

In GVVPT2, the rotation matrix $\mathbf{X}$ is defined in terms of a nonlinear energy shift Δ_i together with a hyperbolic tangent function, which plays the role of a switching function between degenerate and nondegenerate regimes[84]

$$X_{qi} = \frac{\tanh(\Delta_i)}{\Delta_i} H_{qi}$$

$$= \frac{\tanh(\Delta_i)}{\Delta_i} \sum_{m \in L_M} H_{qm} C_{mi},$$

(2.65)

$$\Delta_i = \frac{1}{2}\Big(\varepsilon_q^i - \varepsilon_i^{(0)}\Big) + \frac{1}{2}\sqrt{\Big(\varepsilon_q^i - \varepsilon_i^{(0)}\Big)^2 + 4\sum_{q \in e} H_{qi}^2}.$$

(2.66)

where ε_q^i and $\varepsilon_i^{(0)}$ are the Møller-Plesset-type energies computed from the state-specific one-particle density matrix and state-dependent orbital energies. The elements C_{mi} stem from the transformation matrix $\mathbf{C}_{MP}$ that connects the set of orthonormal eigenvectors of

the unperturbed Hamiltonian in the model space $|\mathbf{\Phi}_P\rangle = \left|\Phi_1, \Phi_2, \dots, \Phi_{N_p}\right\rangle$ to the many-electron basis set $\mathbf{F}_M = \left|F_1, F_2, \dots, F_{N_m}\right\rangle$

$$|\mathbf{\Phi}_P\rangle = |\mathbf{F}_M\rangle \mathbf{C}_{MP}. \tag{2.67}$$

Use of a resolvent in this manner results in ground and excited state potential energy surfaces generated from GVVPT2 calculations that are rigorously continuous and differentiable. Coupling this with an implementation that is inherently spin-adapted and supports both complete and incomplete active spaces, allows GVVPT2 to study challenging problems, such as d- and f-block metal systems.

Although these systems are computationally demanding, applying macroconfigurations, which allow active spaces to be partitioned into an arbitrary number of groups and electrons to be arbitrarily distributed among those groups, reduces this cost while increasing flexibility within the calculation.[85] Configuration spaces of separate macroconfigurations are orthogonal, so the entire configuration space, $L(X)$, induced by a set of macroconfigurations is generated through a direct sum

$$L(X) = L(X_0) \oplus L(X_1) \oplus L(X_2) \oplus \dots \tag{2.68}$$

Within the framework of an Abelian subgroup, each configuration $\boldsymbol{m}$ creates configuration state functions (CSFs) of the same nondegenerate, irreducible representation $\Gamma(\boldsymbol{m})$, so the subspace $L(\boldsymbol{N}; \Gamma, S, M)$ of all the CSFs can be expanded over subspaces $\{l(\boldsymbol{m}; \Gamma(\boldsymbol{m}), S, M)\}_{\boldsymbol{m} \in \kappa(N)}$ given the spatial (Γ) and spin (S, M) symmetries

$$L(\boldsymbol{N};\Gamma,S,M) = \sum_{k=K_{min}^{S}(\boldsymbol{N})}^{K_{max}(\boldsymbol{N})} \sum_{\substack{\boldsymbol{m}\in\kappa(\boldsymbol{N})\\(k(\boldsymbol{m})=k,\Gamma(\boldsymbol{m})=\Gamma)}} \oplus\, l(\boldsymbol{m};\Gamma(\boldsymbol{m}),S,M).$$ (2.69)

Double Group Symmetry

As was discussed in Chapter 1, orbital and spin angular momenta are no longer good quantum numbers with the inclusion of spin-orbit interactions, i.e., l and s are no longer conserved quantities. Rather, the total angular momentum $\boldsymbol{j} = \boldsymbol{l} + \boldsymbol{s}$, which can be an integer or half integer value, is considered in relativistic chemistry. In this spirit, j is substituted for l when considering the character of the representation of a state wavefunction under a symmetry operation.[86] Such operations χ defined by a rotation by an angle α are given by the equation

$$\chi(\alpha) = \frac{\sin\left[\dfrac{(2j+1)\alpha}{2}\right]}{\sin\left(\dfrac{\alpha}{2}\right)}.$$ (2.70)

If instead a proper rotation through an angle of $\alpha + 2\pi$ is considered, then

$$\chi(\alpha + 2\pi) = \frac{\sin\left[\left(\dfrac{2j+1}{2}\right)(\alpha + 2\pi)\right]}{\sin\left[\dfrac{(\alpha + 2\pi)}{2}\right]}$$

$$= \frac{\sin\left[\left(\dfrac{(2j+1)\alpha}{2}\right) + [(2j+1)\pi]\right]}{\sin\left[\left(\dfrac{\alpha}{2}\right) + \pi\right]}.$$ (2.71)

By applying the relation $\sin(a + b) = \sin a \cos b + \cos a \sin b$, and eliminating $\sin n\pi$ ($= 0$) terms, equation 2.70 can be rewritten as

$$\chi(\alpha + 2\pi) = \frac{\sin\left[\frac{(2j + 1)\alpha}{2}\right]\cos[(2j + 1)\pi]}{\sin\left(\frac{\alpha}{2}\right)\cos\pi}$$

$$= (-1)^{2j}\chi(\alpha). \tag{2.72}$$

By analyzing this equation against different j values, it can be seen that

$$j = n \;\rightarrow\; \chi(\alpha + 2\pi) = \chi(\alpha) \tag{2.73}$$

$$j = \frac{n}{2} \;\rightarrow\; \chi(\alpha + 2\pi) = -\chi(\alpha). \tag{2.74}$$

This behavior occurs because state functions are represented as bispinors (the product of an orbital and a spin function) rather than vectors. Therefore, a new symmetry element is defined

$$\bar{E} = \hat{R}(2\pi, n), \tag{2.75}$$

which is a rotation of 2π radians about axis n. In relativistic chemistry, the element $\bar{E}$ is included into the ordinary point groups, leading to the formation of double groups. The double groups then contain twice the number of symmetry elements compared to their single group counterparts, as well as additional irreducible representations (irreps) describing behavior under the symmetry element $\bar{E}$.

    As an example, the $C_{2v}{}^*$ double group is shown in Table 3.1.[87] The double group contain eight symmetry elements: E, $C_2(z)$, $\sigma_v(xz)$, $\sigma_v(yz)$, $\bar{E}$, $C_2(z)\bar{E}$, $\sigma_v(xz)\bar{E}$, and

$\sigma_v(yz)\bar{E}$. The new doubly degenerate irrep E appears in this group, describing the behavior

of functions when $j = \frac{n}{2}$ (fermions). The four original irreps, corresponding to the behavior

of functions when $j = n$ (bosons), remain invariant under the operation of $\bar{E}$. Furthermore,

the cartesian components of a triplet-spin function, s_x, s_y, and s_z, span the B_2, B_1, and A_2

irreps, respectively, whereas the singlet-spin function spans the totally symmetric irrep A_1.

The Kramers pair[88] (α, β) together span the doubly degenerate irrep E. Similar

considerations can be made to generate symmetry tables for other double groups.

Table 2.1. The C_{2v} double group.

C_{2v}^*	E	$\bar{E}$	$C_2(z), C_2(z)\bar{E}$	$\sigma v(xz), \sigma v(xz)\bar{E}$	$\sigma v(yz), \sigma v(yz)\bar{E}$	
A_1	1	1	1	1	1	$\alpha\beta$-$\beta\alpha$
A_2	1	1	1	-1	-1	$R_z, \hat{s}_z, \alpha\beta+\beta\alpha$
B_1	1	1	-1	1	-1	$R_y, \hat{s}_y, \alpha\alpha+\beta\beta$
B_2	1	1	-1	-1	1	$R_x, \hat{s}_x, \alpha\alpha$-$\beta\beta$
E	2	-2	0	0	0	(α, β)

Following the procedure presented by Visscher,[86] construction of the symmetry

functions $\chi_i^{\Gamma_1,\Gamma_2}$, where Γ_1 and Γ_2 are irreps for an associated symmetry group, for the

fermionic irreps can be done by introducing a new character projection operator

$$\hat{P}^E = \frac{1}{2}\left(\hat{E} - \hat{R}\right). \tag{2.76}$$

By considering a product of character projection operators, the symmetry functions for the

bosonic irreps can be projected out from a trial function. These symmetry functions are

used to define the matrix representations of the operations of their corresponding double group.

The matrix representations may differ in phase of the off-diagonal elements. Multiplying the symmetry functions by an appropriate phase factor will standardize the representations, leading to reduction in cost for double group symmetry-adapted relativistic calculations.

In order to assure that the integrals are real, a constraint is imposed on the basis functions, requiring them to be Kramers pairs. Applying the anti-unitary Kramers operator $\widehat{K}$ to a symmetry function of one bosonic irrep transforms it according to the relation

$$\widehat{K}\chi_i^{E,\Gamma'} = \chi_i^{E,\Gamma''}, \tag{2.77}$$

$$\widehat{K}\chi_i^{E,\Gamma''} = -\chi_i^{E,\Gamma'}, \tag{2.78}$$

where Γ' and Γ'' are bosonic irreps. If the Kramers operator is applied to an integral over these functions, two effects may result: either (1) the functions are transformed according to the above relation, or (2) the value of the integral is changed into its complex conjugate. Performing a symmetry operation on the same integral has the same effect as the Kramers operator, but instead of changing the value to its complex conjugate, the integral retains the original real value. Since these operations yield the same result, the complex-valued integral and the real-valued integral must be equal. Therefore, the integrals must be real.

The symmetry functions of groups with higher-order symmetry can be treated using a product of two character projection operators: one for the highest point group irrep, and

32

one for the highest Abelian subgroup irrep to resolve the degeneracy of the highest irrep. The group chains and their correspondence of representations used in constructing these symmetry functions are given in Table 3.2.[86] Note that the same chains are used for groups that are direct products of the groups listed with the inversion group.

Table 2.2. Group chains used in the construction of symmetry functions.

Point Group	Irrep	Abelian subgroup	Irrep
$D_2{}^*$	E	$C_2{}^*$	E', E''
$C_{2v}{}^*$	E	$C_2{}^*$	E', E''
$C_{4v}{}^*$	E_1	$C_4{}^*$	E_1', E_1''
	E_2		E_2', E_2''
$D_4{}^*$	E_1	$C_4{}^*$	E_1', E_1''
	E_2		E_2', E_2''
$D_{2d}{}^*$	E_1	$S_4{}^*$	E_1', E_1''
	E_2		E_2', E_2''
$T_d{}^*$	E_1	$S_4{}^*$	E_1', E_1''
	E_2		E_2', E_2''
	U		E_1', E_1'', E_2', E_2''
O^*	E_1	$C_4{}^*$	E_1', E_1''
	E_2		E_2', E_2''
	U		E_1', E_1'', E_2', E_2''
T^*	E	$C_3{}^*$	E', E''
	U'		B, E'
	U''		B, E''
T^*	E	$C_2{}^*$	E', E''
	U		E', E''

Implementation of these double groups can be accomplished following a rather simple procedure. First, the highest order Abelian group is considered to produce orthogonal symmetry function, using character projection operators defined by corresponding pairs of irreps (Γ, Γ'). A spin orbital is chosen as a trial function from which basis functions for each of the irreps are projected. Operating on these basis functions with $\widehat{K}$ gives the Kramers partner for each of these basis functions, and representation matrices for each of the symmetry operations within that group are defined by these Kramers pairs. Phase factors are included where appropriate in order to maintain consistency in the matrix representations.

In the case that a particular irrep is spanned more than once by a group of symmetry-related trial functions, the Kramers partner is generated by operating on the basis function with a symmetry element of the group rather than $\widehat{K}$. This gives a proper representation of the matrices. It is found that, in general,

$$\widehat{K}\chi_i^{E,\Gamma'} = \sum_j U_{ij}\chi_j^{E,\Gamma''}, \tag{2.79}$$

$$\widehat{K}\chi_i^{E,\Gamma''} = -\sum_j U_{ij}^T\chi_j^{E,\Gamma''}, \tag{2.80}$$

where U is a unitary matrix. When U is not the unit matrix, a transformation of the initial symmetry functions $\chi_i^{E,\Gamma'}$ and $\chi_i^{E,\Gamma''}$ by $U^{\frac{1}{2}}$ is necessary. This transformation does not

34

change the representation matrices, but instead provides a new satisfactory set of functions and gives real integrals.[86]

By following this process, no other special procedures need to be implemented in order to treat the objects within this formulation. The same real algebra is followed, and, therefore, the same conditions that were imposed on the basis functions are fulfilled. As symmetry exploitation leads to reduction in computational cost, incorporation of double group symmetry is a decent addition to any relativistic method.

CHAPTER III

SPIN-DEPENDENT RELATIVISTIC GVVPT2

The Two-Electron Spin-Orbit Integrals

In order to derive the expressions for the relativistic integrals to be evaluated, consider the Breit-Pauli (BP) Hamiltonian, which is separated into one- and two-electron parts

$$\hat{H}_{SO} = \hat{H}_{SO}(1) + \hat{H}_{SO}(1,2)$$

$$= \frac{e^2\hbar}{2m^2c^2}\left\{\sum_k\sum_\alpha \frac{Z_\alpha}{r_{\alpha k}^3}[r_{\alpha k}\cdot s(k)] - \sum_{k,j\neq k} r_{kj}^{-3}[r_{kj}\times p_k]\cdot[s(k)+2s(j)]\right\}, \qquad (3.1)$$

where

$$r_{\alpha k} = r_k - r_\alpha, \qquad r_{kj} = r_k - r_j. \qquad (3.2)$$

The indices k, j represent the electrons, and α represents the nucleus. Now, the one- (which will be denoted as $L(k,\alpha)$) and two-electron (which will be denoted as $J(k,j)$) operators in the BP Hamiltonian can be defined

$$L_m(k,\alpha) = \left[\frac{Z_\alpha}{r_{\alpha k}^3}(r_{\alpha k}\times p_k)\right]_m$$

$$= \frac{\hbar}{i}\left[\frac{Z_\alpha}{r_{\alpha k}^3}(r_{\alpha k}\times \nabla_k)\right]_m, \qquad (3.3)$$

$$J_q(k,j) = \left[\left(\frac{r_{kj}}{r_{kj}^3} \times p_k \right) \right]_m$$

$$= \frac{\hbar}{i} \left[\frac{1}{r_{kj}^3} \left(r_{kj} \times \nabla_k \right) \right]_m,$$

(3.4)

where $m = x, y, z$.

The one-electron relativistic integrals have previously been derived and implemented into UNDMOL,[76] so this discussion will focus on the two-electron relativistic integrals. Following the method by King and Furlani,[89] first (arbitrarily) consider the z-component of the two-electron operator

$$J_z(k,j) = \frac{\hbar}{i} \left[\frac{1}{r_{kj}^3} \left(r_{kj} \times \nabla_k \right) \right]_z$$

$$\equiv J_0(k,j).$$

(3.5)

Carrying out the cross product yields

$$\left(r_{kj} \times \nabla_k \right) = \begin{vmatrix} \hat{x} & \hat{y} & \hat{z} \\ (x_k - x_j) & (y_k - y_j) & (z_k - z_j) \\ \dfrac{\partial}{\partial x_k} & \dfrac{\partial}{\partial y_k} & \dfrac{\partial}{\partial z_k} \end{vmatrix}$$

$$= \begin{pmatrix} (y_k - y_j)\dfrac{\partial}{\partial z_k} - (z_k - z_j)\dfrac{\partial}{\partial y_k} \\ (z_k - z_j)\dfrac{\partial}{\partial x_k} - (x_k - x_j)\dfrac{\partial}{\partial z_k} \\ (x_k - x_j)\dfrac{\partial}{\partial y_k} - (y_k - y_j)\dfrac{\partial}{\partial x_k} \end{pmatrix}.$$

(3.6)

So the expression for the z-component becomes

$$J_z(k,j) = \frac{\hbar}{i}\left[\frac{1}{r_{kj}^3}\left((x_k - x_j)\frac{\partial}{\partial y_k} - (y_k - y_j)\frac{\partial}{\partial x_k}\right)\right]. \tag{3.7}$$

Using this form of the operator, the expression for the two-electron spin-orbit integrals can be obtained. Similar to the electron repulsion integrals (ERIs), a four-center integral is constructed

$$\langle ab|J_z|cd\rangle = \langle a(k)b(j)|J_z(k,j)|c(k)d(j)\rangle$$

$$= \iint \varphi_a(k)\varphi_b(j)\left[\frac{\hbar}{i}\left(\frac{1}{r_{kj}^3}\left((x_k - x_j)\frac{\partial}{\partial y_k}\right.\right.\right.$$

$$\left.\left.\left. - (y_k - y_j)\frac{\partial}{\partial x_k}\right)\right)\right]\varphi_c(k)\varphi_d(j)\,dz_k\,dz_j$$

$$= \frac{\hbar}{i}\iint \frac{1}{r_{kj}^3}\varphi_a(k)\varphi_b(j)\left[(x_k - x_j)\frac{\partial}{\partial y_k}\right.$$

$$\left. - (y_k - y_j)\frac{\partial}{\partial x_k}\right]\varphi_c(k)\varphi_d(j)\,dz_k\,dz_j$$

$$= \frac{\hbar}{i}\left[\iint \frac{(x_k - x_j)}{r_{kj}^3}\varphi_a(k)\varphi_b(j)\frac{\partial}{\partial y_k}\varphi_c(k)\varphi_d(j)\,dz_k\,dz_j\right.$$

$$\left. - \iint \frac{(y_k - y_j)}{r_{kj}^3}\varphi_a(k)\varphi_b(j)\frac{\partial}{\partial x_k}\varphi_c(k)\varphi_d(j)\,dz_k\,dz_j\right]. \tag{3.8}$$

While evaluating the integrals in terms of derivative ERIs would be sufficient in determining the two-electron spin-orbit integrals, the expression can be further derived to express these integrals in terms of the ERIs themselves. Since the ERIs are computed in a

quantum chemical calculation, this would bypass the need to evaluate derivative ERIs simply to compute the two-electron spin-orbit integrals.

The basis functions φ_i are defined as generic Gaussians

$$\varphi_\alpha(k) = \varphi_\alpha\big(\vec{r}_k, \zeta_\alpha, \vec{\alpha}, \vec{\mathcal{A}}\big)$$

$$= (x - \mathcal{A}_x)^{\alpha_x}\big(y - \mathcal{A}_y\big)^{\alpha_y}(z - \mathcal{A}_z)^{\alpha_z}\exp\left[-\zeta_\alpha\big(\vec{r}_k - \vec{\mathcal{A}}\big)^2\right]. \qquad (3.9)$$

The derivatives of these functions can then be expressed as

$$\frac{\partial}{\partial r_i}\varphi_\alpha(k) = N_m(\vec{\alpha})\varphi_\alpha\big(\vec{r}_k, \zeta_\alpha, \vec{\alpha} - 1_m, \vec{\mathcal{A}}\big) - 2\zeta_\alpha\varphi_\alpha\big(\vec{r}_k, \zeta_\alpha, \vec{\alpha} + 1_m, \vec{\mathcal{A}}\big)$$

$$= N_m(\vec{\alpha})\varphi_{\alpha-1_m}(k) - 2\zeta_\alpha\varphi_{\alpha+1_m}(k), \qquad (3.10)$$

where $N_m(\vec{\alpha}) = \alpha_m$. By letting $\tilde{f}_m(\vec{\alpha}) = N_m(\vec{\alpha})\varphi_{\alpha-1_m}(k) - 2\zeta_\alpha\varphi_{\alpha+1_m}(k)$, the two-electron spin-orbit integrals can be re-expressed as

$$\langle ab|J_z|cd\rangle = \frac{\hbar}{i}\left[\iint \frac{(x_k - x_j)}{r_{kj}^3}\varphi_a(k)\varphi_b(j)\big[\tilde{f}_y(\vec{c})\big]\varphi_d(j)\,dz_k\,dz_j\right.$$

$$\left. - \iint \frac{(y_k - y_j)}{r_{kj}^3}\varphi_a(k)\varphi_b(j)\big[\tilde{f}_x(\vec{c})\big]\varphi_d(j)\,dz_k\,dz_j\right]. \qquad (3.11)$$

It is sufficient to say (and can be shown) that

$$\int \frac{(m_k - m_j)}{r_{kj}^3}\varphi_a(k)\varphi_c(k)\,dm_k$$

$$= \int \frac{1}{r_{kj}}\big[\tilde{f}_m(\vec{a})\big]\varphi_c(k)\,dm_k + \int \frac{1}{r_{kj}}\varphi_a(k)\big[\tilde{f}_m(\vec{c})\big]\,dm_k, \qquad (3.12)$$

so, by defining the ERI as

39

$$\langle ab|cd\rangle = \iint \varphi_a(k)\varphi_b(j)\frac{1}{r_{kj}}\varphi_c(k)\varphi_d(j)\,dr_k\,dr_j, \qquad (3.13)$$

and defining changes to the angular momentum of the components as

$$\langle a_{\pm m}b|cd\rangle = \iint \varphi_{a\pm 1_m}(k)\,\varphi_b(j)\frac{1}{r_{kj}}\varphi_c(k)\varphi_d(j)\,dr_k\,dr_j, \qquad (3.14)$$

the two-electron spin-orbit expression given in equation (3.11) can be rewritten

$$\langle ab|J_z|cd\rangle = \frac{\hbar}{i}\Big\{ N_x(\vec{a})N_y(\vec{c})\langle a_{-x}b|c_{-y}d\rangle - 2\zeta_a N_y(\vec{c})\langle a_{+x}b|c_{-y}d\rangle$$

$$- 2\zeta_c N_x(\vec{a})\langle a_{-x}b|c_{+y}d\rangle + 4\zeta_a\zeta_c\langle a_{+x}b|c_{+y}d\rangle$$

$$- N_y(\vec{a})N_x(\vec{c})\langle a_{-y}b|c_{-x}d\rangle + 2\zeta_a N_x(\vec{c})\langle a_{+y}b|c_{-x}d\rangle$$

$$+ 2\zeta_c N_y(\vec{a})\langle a_{-y}b|c_{+x}d\rangle - 4\zeta_a\zeta_c\langle a_{+y}b|c_{+x}d\rangle$$

$$+ N_x(\vec{c})N_y(\vec{c})\langle ab|c_{-x,-y}d\rangle - 2\zeta_c N_y(\vec{c})\langle ab|c_{+x,-y}d\rangle$$

$$- 2\zeta_c N_x(\vec{c})\langle ab|c_{-x,+y}d\rangle + 4\zeta_c^2\langle ab|c_{+x,+y}d\rangle$$

$$- N_x(\vec{c})N_y(\vec{c})\langle ab|c_{-x,-y}d\rangle + 2\zeta_c N_y(\vec{c})\langle ab|c_{+x,-y}d\rangle$$

$$+ 2\zeta_c N_x(\vec{c})\langle ab|c_{-x,+y}d\rangle - 4\zeta_c^2\langle ab|c_{+x,+y}d\rangle\Big\}. \qquad (3.15)$$

The last eight terms of this expression cancel out, which, after rearranging, yields

$$\langle ab|J_z|cd\rangle = \frac{\hbar}{i}\{N_x(\vec{a})N_y(\vec{c})\langle a_{-x}b|c_{-y}d\rangle - N_y(\vec{a})N_x(\vec{c})\langle a_{-y}b|c_{-x}d\rangle$$

$$+ 2\zeta_a[N_x(\vec{c})\langle a_{+y}b|c_{-x}d\rangle - N_y(\vec{c})\langle a_{+x}b|c_{-y}d\rangle]$$

$$+ 2\zeta_c[N_y(\vec{a})\langle a_{-y}b|c_{+x}d\rangle - N_x(\vec{a})\langle a_{-x}b|c_{+y}d\rangle]$$

$$+ 4\zeta_a\zeta_c[\langle a_{+x}b|c_{+y}d\rangle - \langle a_{+y}b|c_{+x}d\rangle]\}. \tag{3.16}$$

This derivation was carried out in "physicist notation" and must be converted to "chemists notation." This can be achieved using the relation

$$\langle ik|jl\rangle \equiv (ij|kl), \tag{3.17}$$

since

$$\langle ik|jl\rangle = \iint \varphi_i^*(1)\varphi_k^*(2)\frac{1}{r_{12}}\varphi_j(1)\varphi_l(2)\,dr_1\,dr_2 \tag{3.18}$$

and

$$(ij|kl) = \iint \varphi_i^*(1)\varphi_j(1)\frac{1}{r_{12}}\varphi_k^*(2)\varphi_l(2)\,dr_1\,dr_2. \tag{3.19}$$

Thus, the final expression for the z-component of the two-electron spin-orbit integrals is given by

$$(ab|J_z|cd) = \frac{\hbar}{i}\{N_x(\vec{a})N_y(\vec{b})(a_{-x}b_{-y}|cd) - N_y(\vec{a})N_x(\vec{b})(a_{-y}b_{-x}|cd)$$

$$+ 2\zeta_a[N_x(\vec{b})(a_{+y}b_{-x}|cd) - N_y(\vec{b})(a_{+x}b_{-y}|cd)]$$

$$+ 2\zeta_b[N_y(\vec{a})(a_{-y}b_{+x}|cd) - N_x(\vec{a})(a_{-x}b_{+y}|cd)]$$

$$+ 4\zeta_a\zeta_b[(a_{+x}b_{+y}|cd) - (a_{+y}b_{+x}|cd)]\}. \tag{3.20}$$

A similar derivation can be done for the *x*- and *y*-components of the two-electron operator. The resulting equations are given by

$$(ab|J_x|cd) = \frac{\hbar}{i}\{N_y(\vec{a})N_z(\vec{b})(a_{-y}b_{-z}|cd) - N_z(\vec{a})N_y(\vec{b})(a_{-z}b_{-y}|cd)$$

$$+ 2\zeta_a[N_y(\vec{b})(a_{+z}b_{-y}|cd) - N_z(\vec{b})(a_{+y}b_{-z}|cd)]$$

$$+ 2\zeta_b[N_z(\vec{a})(a_{-z}b_{+y}|cd) - N_y(\vec{a})(a_{-y}b_{+z}|cd)]$$

$$+ 4\zeta_a\zeta_b[(a_{+y}b_{+z}|cd) - (a_{+z}b_{+y}|cd)]\} \tag{3.21}$$

and

$$(ab|J_y|cd) = \frac{\hbar}{i}\{N_z(\vec{a})N_x(\vec{b})(a_{-z}b_{-x}|cd) - N_x(\vec{a})N_z(\vec{b})(a_{-x}b_{-z}|cd)$$

$$+ 2\zeta_a[N_z(\vec{b})(a_{+x}b_{-z}|cd) - N_x(\vec{b})(a_{+z}b_{-x}|cd)]$$

$$+ 2\zeta_b[N_x(\vec{a})(a_{-x}b_{+z}|cd) - N_z(\vec{a})(a_{-z}b_{+x}|cd)]$$

$$+ 4\zeta_a\zeta_b[(a_{+z}b_{+x}|cd) - (a_{+x}b_{+z}|cd)]\}. \tag{3.22}$$

Within this derivation, the spin-orbit integrals are constructed by coordinate through combinations of ERIs of the other coordinates, with the angular momentum of the components of the ERIs is augmented or diminished by one with respect to the corresponding spin-orbit integral. Therefore, only the ERIs must be produced in order to generate the correct auxiliary functions to be used for the construction of the two-electron spin-orbit integrals, which are computed at the beginning of the calculation. Thus, by retrieving the corresponding ERIs, the two-electron spin-orbit integrals may be constructed at any point after the integrals evaluation during a calculation.

Construction of the sf-X2C+so-DKH3 Hamiltonian

After the two-electron spin-orbit integrals have been computed, the spin-orbit Hamiltonian can be constructed from them. Using this Hamiltonian directly is computationally demanding. Rather, as found in a survey of relativistic Hamiltonians by Liu et al., an X2C treatment of the spin-free terms with a DKH3 treatment of the spin-dependent terms is most practical, resulting in a sf-X2C+so-DKH3 Hamiltonian.[78] This Hamiltonian can be constructed following the general ansatz outlined in Chapter 2. The resultant Hamiltonian in equation (2.42) must then be block-diagonalized, which can be achieved through a series of DKH-like unitary transformations. This results in a Hamiltonian of the form

$$\mathbf{h}_+ = \mathbf{E}_{+,0} + \mathbf{E}_{+,1} + \mathbf{E}_{+,2} + \mathbf{E}_{+,3}, \tag{3.23}$$

which here is truncated at third-order in compliance with the results of Liu et al. The first term corresponds to the spin-free part, with the remaining three terms corresponding to the spin-dependent part. Each term can be expressed as

$$\mathbf{E}_{+,0} = \mathbf{h}_{+,sf} = \mathbf{R}_{+,0}^\dagger \tilde{\mathbf{L}}_{+,0}^{NESC} \mathbf{R}_{+,0}, \tag{3.24}$$

$$\mathbf{E}_{+,1} = \frac{\alpha^2}{4} \mathbf{R}_{+,0}^\dagger \mathbf{X}_0^\dagger \mathbf{W}_{sd} \mathbf{X}_0 \mathbf{R}_{+,0}, \tag{3.25}$$

$$\mathbf{E}_{+,2} = \frac{1}{\alpha^2} \left(\mathbf{W}_1 \mathbf{T}^{-1} \mathbf{O}_1^\dagger + c.c. \right), \tag{3.26}$$

$$\mathbf{E}_{+,3} = \frac{1}{\alpha^2} \left(\mathbf{W}_1 \mathbf{T}^{-1} \mathbf{O}_2^\dagger + c.c. \right), \tag{3.27}$$

43

where

$$\tilde{\mathbf{L}}_{+,0}^{NESC} = \mathbf{V} + \mathbf{T}\mathbf{X}_0 + \mathbf{X}_0^\dagger\mathbf{T} + \mathbf{X}_0^\dagger\left(\frac{\alpha^2}{4}\mathbf{W}_{sf} - \mathbf{T}\right)\mathbf{X}_0, \tag{3.28}$$

$$\mathbf{W}_1 = \frac{\alpha^2}{2}\mathbf{S}\mathbf{C}_{+,0}\mathbf{w}_1\mathbf{C}_{-,0}^\dagger\mathbf{T}, \tag{3.29}$$

$$[\mathbf{w}_1]_{pq} = -\frac{[\mathbf{o}_1]_{pq}}{\left[E_{-,0}\right]_q - \left[E_{+,0}\right]_p}, \qquad \mathbf{o}_1 = \mathbf{C}_{+,0}^\dagger\mathbf{O}_1\mathbf{C}_{-,0}, \tag{3.30}$$

$$\mathbf{O}_1 = \frac{\alpha^2}{4}\mathbf{R}_{+,0}^\dagger\mathbf{X}_0^\dagger\mathbf{W}_{sd}\mathbf{R}_{-,0}, \tag{3.31}$$

$$\mathbf{O}_2 = \frac{2}{\alpha^2}\mathbf{W}_1\mathbf{T}^{-1}\mathbf{E}_{-,1} - \mathbf{E}_{+,1}\mathbf{S}^{-1}\mathbf{W}_1, \tag{3.32}$$

$$\mathbf{E}_{-,1} = \frac{\alpha^2}{4}\mathbf{R}_{-,0}^\dagger\mathbf{W}_{sd}\mathbf{R}_{-,0}. \tag{3.33}$$

with $\mathbf{R}_{+,0}$, $\mathbf{R}_{-,0}$ defined by equations (2.34) and (2.35), respectively, the decoupling matrix $\mathbf{X}_0$, defined by equation (2.27), and the coefficient matrix $\mathbf{C}_{+,0}$ defined by equation (2.43), whereas $\mathbf{C}_{-,0}$ is defined by

$$\mathbf{C}_{-,0} = \mathbf{R}_-^{-1}\mathbf{B}_-. \tag{3.34}$$

By applying the Dirac identity, each of the expressions for $\mathbf{E}_{+,1}$, $\mathbf{E}_{+,2}$, and $\mathbf{E}_{+,3}$ can be written in the form $\mathbf{E}_{+,k} = \mathbf{E}_{+,k}^{sf} + i\vec{\sigma}\cdot\mathbf{E}_{+,k}^{sd}$. Therefore, for $\mathbf{E}_{+,2}$, the expressions for the spin-free and spin-dependent parts become

$$\mathbf{E}_{+,2}^{sf} = \frac{1}{\alpha^2}\left(\vec{\mathbf{W}}_1\cdot\mathbf{T}^{-1}\vec{\mathbf{O}}_1^T + \vec{\mathbf{O}}_1\cdot\mathbf{T}^{-1}\vec{\mathbf{W}}_1^T\right), \tag{3.35}$$

$$\mathbf{E}_{+,2}^{sd} = \frac{1}{\alpha^2}\left(\overrightarrow{\mathbf{W}}_1 \times \mathbf{T}^{-1}\overrightarrow{\mathbf{O}}_1^T + \overrightarrow{\mathbf{O}}_1 \times \mathbf{T}^{-1}\overrightarrow{\mathbf{W}}_1^T\right). \tag{3.36}$$

Similarly, $\mathbf{O}_2$ can be further separated into spin-free and spin-dependent parts

$$\mathbf{O}_2^{sf} = -\left(2c^2\overrightarrow{\mathbf{W}}_1 \cdot \mathbf{T}^{-1}\overrightarrow{\mathbf{E}}_{-,1} - \overrightarrow{\mathbf{E}}_{+,1} \cdot \mathbf{S}^{-1}\overrightarrow{\mathbf{W}}_1\right), \tag{3.37}$$

$$\mathbf{O}_2^{sd} = -\left(2c^2\overrightarrow{\mathbf{W}}_1 \times \mathbf{T}^{-1}\overrightarrow{\mathbf{E}}_{-,1} - \overrightarrow{\mathbf{E}}_{+,1} \times \mathbf{S}^{-1}\overrightarrow{\mathbf{W}}_1\right), \tag{3.38}$$

so that the spin-free and spin-dependent parts of $\mathbf{E}_{+,3}$ can be expressed as

$$\mathbf{E}_{+,3}^{sf} = \frac{1}{\alpha^2}\left(\overrightarrow{\mathbf{W}}_1 \cdot \mathbf{T}^{-1}\overrightarrow{\mathbf{O}}_2^{sd,T} + \overrightarrow{\mathbf{O}}_2^{sd} \cdot \mathbf{T}^{-1}\overrightarrow{\mathbf{W}}_1^T\right), \tag{3.39}$$

$$\begin{aligned}\mathbf{E}_{+,3}^{sd} = \frac{1}{\alpha^2}\Big(&\overrightarrow{\mathbf{W}}_1 \mathbf{T}^{-1}\mathbf{O}_2^{sf,T} - \mathbf{O}_2^{sf}\mathbf{T}^{-1}\overrightarrow{\mathbf{W}}_1^T + \overrightarrow{\mathbf{W}}_1 \times \mathbf{T}^{-1}\overrightarrow{\mathbf{O}}_2^{sd,T} \\ &+ \overrightarrow{\mathbf{O}}_2^{sd} \times \mathbf{T}^{-1}\overrightarrow{\mathbf{W}}_1^T\Big).\end{aligned} \tag{3.40}$$

Thus, the sf-X2C+so-DKH3 Hamiltonian can be written in a fully spin-separated form

$$\mathbf{h}_+ = \left(\mathbf{E}_{+,0} + \mathbf{E}_{+,2}^{sf} + \mathbf{E}_{+,3}^{sf}\right) + i\vec{\sigma} \cdot \left(\overrightarrow{\mathbf{E}}_{+,1} + \overrightarrow{\mathbf{E}}_{+,2}^{sd} + \overrightarrow{\mathbf{E}}_{+,3}^{sd}\right). \tag{3.41}$$

Spin-Dependent GVVPT2

While there are several different ways of incorporating relativistic effects into quantum chemical calculations, defining the relativistic Hamiltonian according to equation (3.41) allows the spin-dependent relativistic effects to be included into the calculations perturbatively. Since the mathematical details of this approach have been presented previously in this thesis, a description of the computational details of this method, as well as an alternative method (relativistic corrections to the Hamiltonian from the elements of the transition one-particle density matrix), is discussed in the following paragraphs.

45

In order to generate the transition one-particle density matrix, determinants must be calculated from configuration state functions (CSFs) of the system under consideration. The CSFs are retrieved at the end of the calculation, since the relativistic corrections can be introduced as a perturbative correction. The step vectors, as promulgated by Shavitt, for each CSF are stored in an array and used as input to a Harter-Patterson routine[90] to convert the strings into determinants. The corresponding coefficients of the CSFs are also stored in an array to be used later. Once the Harter-Patterson routine calculates the determinants and amplitudes from the step vectors, elements of the transition one-particle density matrix γ can then be found from the equation

$$\gamma_{ij}^{12} = \sum_{mn} \left(\sum_I c_I^1 a_I^m \right) \langle d_m | e_{ij} | d_n \rangle \left(\sum_J c_J^2 a_J^n \right) \tag{3.42}$$

where c_N^x are the coefficients of the corresponding CSFs, $a_{N'}^{x'}$ are amplitudes of the determinants $d_{x'}$, and e_{ij} is determined from the equation

$$e_{ij} = X_{i\alpha}^\dagger X_{j\alpha} + X_{i\beta}^\dagger X_{j\beta}. \tag{3.43}$$

This matrix can then be used to make corrections to the Hamiltonian to account for low-order relativistic effects.

While this method provides a more quick and simple way to incorporate low-order relativistic effects, higher-order effects that have a significant impact on the overall energy are missed. A way to improve on this method is to make use of the two-electron spin-orbit interactions, as is done in this research and previously described. The arithmetic describing

46

the evaluation of the two-electron spin-orbit integrals, the X2C method, and the AMFI approximation is discussed in detail in the previous chapters of this thesis. Therefore, the following discussion will describe more of the computational details.

The two-electron spin-orbit integrals are constructed from combinations of electron repulsion integrals (ERIs). Therefore, these integrals can be evaluated on the fly at any time during a calculation as long as the ERIs have been constructed previously. Since the relativistic effects are considered as a perturbation to the Hamiltonian, they will be included at the end of the calculation, which is when the spin-orbit integrals will be evaluated. This way, the integrals can remain in the $L2$ cache during the calculation, allowing for fast access speeds while being large enough for storage purposes.

The two-electron spin-orbit integrals are evaluated in a similar way to the ERIs. Loops are arranged so that the integrals are stored as a row-packed array, beginning with $\langle 00|J|00\rangle$, where J is the spin-orbit operator, and incrementing indices in reverse order (i.e., for $\langle ij|J|kl\rangle$, the loop for l is the inner-most loop, and the loop for i is the outer-most loop). The integrals are constructed coordinate-wise based on the arithmetic outlined in equations (3.20), (3.21), and (3.22) and placed into a structure which identifies the separate indices and associated coordinate-based integral values. After evaluating these integrals, basis function contributions to the integrals, beginning with the left most index, are computed in the same manner as the integral evaluations. A flow diagram demonstrating this procedure is shown in Figure 3.1.
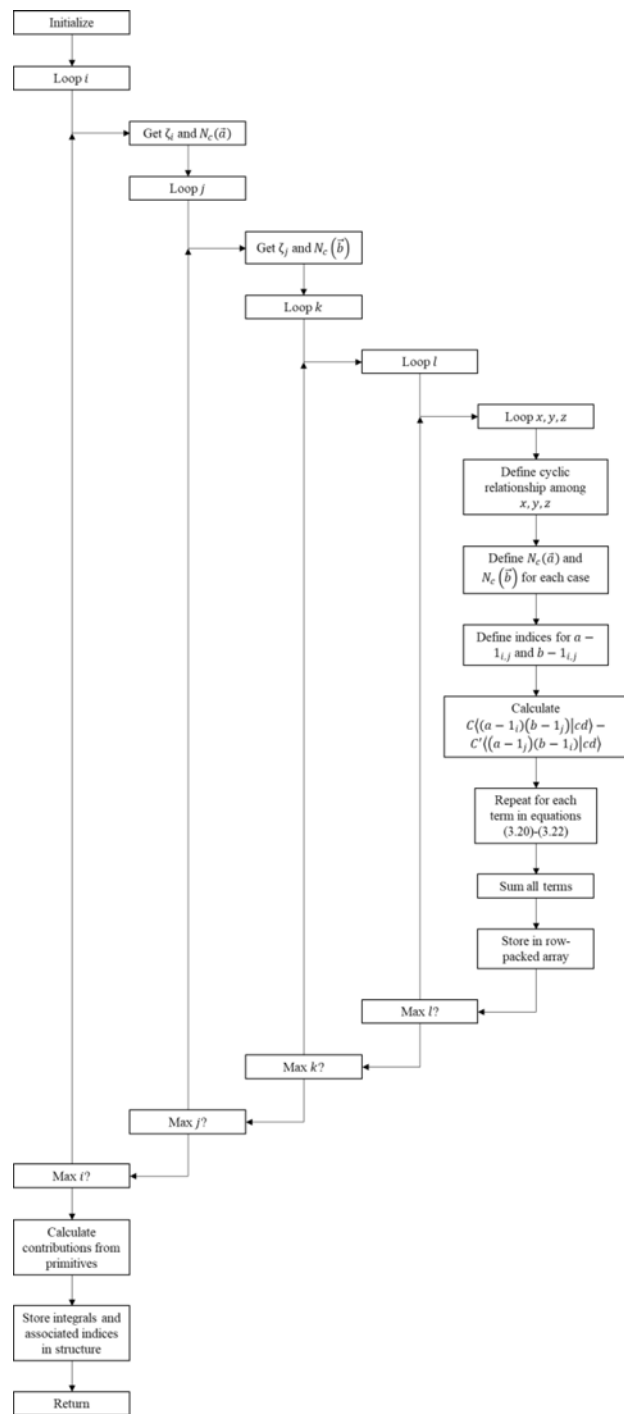
Figure 3.1. Flow diagram for calculating the two-electron spin-orbit integrals.

Using the two-electron spin-orbit integrals directly in a quantum chemical calculation demand significant memory space and time. The AMFI approximation serves as a suitable approximation of the relativistic effects. This method captures the significant two-electron relativistic contributions while reducing time and memory requirements by contracting the two-electron integrals against elements of the one-particle density matrix. Mathematical details about the AMFI approximation are described in Chapter 2 of this thesis.

The elements of the AMFI approximated Hamiltonian are computed by combining one-electron relativistic integrals with the two-electron integrals contracted against the elements of the one-particle density matrix based on separate cartesian coordinates. The loops for the indices are set up so that k is the inner-most loop, and i is the outer-most loop. The set of indices for each of the two-electron integrals used in the evaluation of the Hamiltonian elements are defined within the k-loop. The appropriate integrals are then combined according to (2.60) and contracted against the respective element of the one-particle density matrix. The result is then combined with the corresponding one-electron integral and stored in a row-packed array, similar to the storage of the two-electron integrals. The resulting effective one-electron Hamiltonian provides a reasonable approximation to the relativistic contributions to the system that captures the two-electron

49

interactions, while significantly reducing computational cost by storing the values within the *L2* cache, requiring less dedicated memory necessary for the calculations. A flow diagram detailing the AMFI approximation procedure is shown in Figure 3.2.
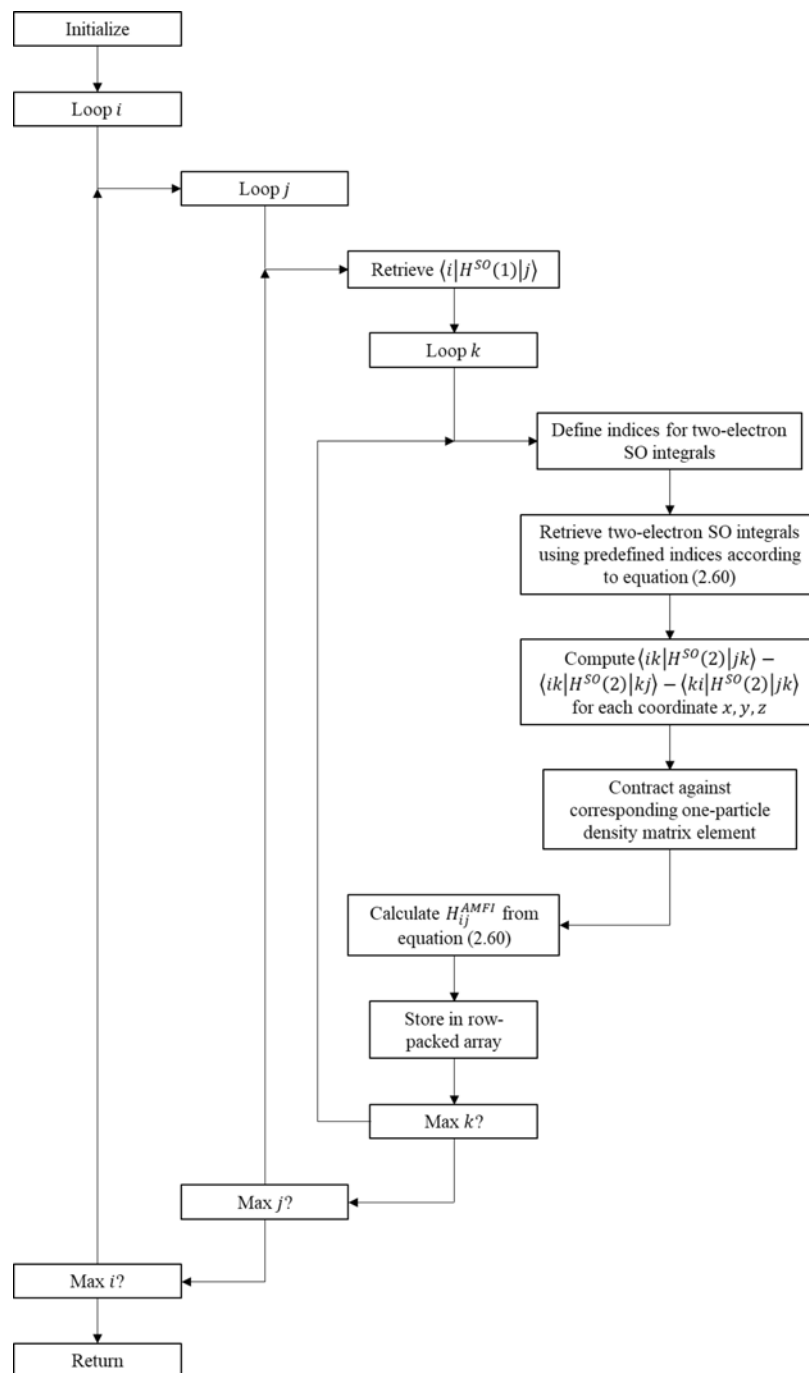
Figure 3.2. Flow diagram for calculating elements of the effective one-electron Hamiltonian generated by the AMFI approximation.

51

By applying this Hamiltonian as a perturbative correction within the calculation, a relativistically accurate description of the system under consideration with chemically accurate results will be obtained. The result of this research can be applied to a wide variety of chemical systems that exhibit significant two-electron spin-orbit effects, in particular, lanthanide dimer systems, as presented in the following chapters of this thesis.

The ansatz outlined in this chapter will produce an electronic structure theory method that satisfies the two main challenges faced by computational approaches for chemical systems containing heavy atoms; (i) scalar- and spin-orbit relativistic effects are accounted for in an accurate and efficient manner through the use of the sf-X2C+so-DKH3 Hamiltonian, and (ii) dynamic and nondynamic electron correlation are treated accurately within GVVPT2, to which this relativistic Hamiltonian will be applied. This relativistic variant of multireference perturbation theory will allow systems containing heavy elements to be studied with the capability of producing chemically accurate results. Such systems under consideration that have applications to single molecule magnets and quantum bits are the d- and f-block metal dimers and trimers. The following chapters in this dissertation provide a theoretical investigation on a few select systems that have gained considerable interest for use in these applications: the gadolinium dimer Gd_2 (Chapter 4), the dysprosium dimer Dy_2 (Chapter 5), and the scandium trimer Sc_3 (Chapter 6).

CHAPTER IV

RELATIVISTIC GVVPT2 STUDY OF GROUND AND LOW-LYING EXCITED

STATES OF THE GADOLINIUM DIMER

Introduction

Recent advances in single molecule magnet (SMM) technology has sparked interest within the chemistry community, both with experimentalists and theoreticians. These materials contain a metallic-based core with large magnetic moments surrounded by nonmetallic ligands. Several studies have focused around SMMs with gadolinium-based cores, showing them to be among some of the more promising candidates for these types of materials.

The gadolinium atom has a ground state electronic configuration of $[Xe]4f^7 5d^1 6s^2$ (shown in Figure 4.1).[91] Each of the seven f electrons as well as the single d electron remain unpaired in the ground state, which results in an atomic term symbol of $^9D_2$, giving it the highest spin multiplicity of any ground state atom in the periodic table.
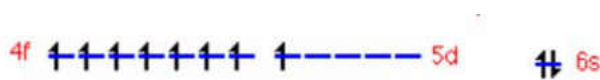
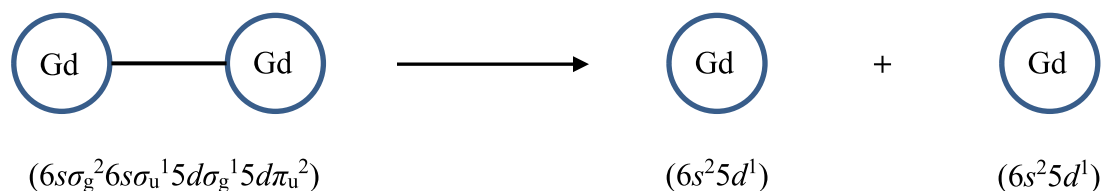**Figure 4.1.** Valence electronic configuration of the Gadolinium atom.

This high spin multiplicity, along with a relatively large effective magnetic moment ($\mu_B^{eff} \approx 6.5$), makes it highly attractive for use in magnetic applications.

53

Gadolinium has recently been studied as a dimer, Gd_2. Electron spin resonance (ESR) spectroscopy has shown that the spectral lines of Gd_2 must be fitted to an $S = 9$ Hamiltonian.[69] This implies that the ground state of Gd_2 contains 18 unpaired electrons which are ferromagnetically coupled, including the 14 electrons of the inner $4f$ shell. Therefore, the ground state (valence and sub-valence) electronic configuration of Gd_2 is (most sensibly) $(4f^7)(4f^7)6s\sigma_g^2 6s\sigma_u^1 5d\sigma_g^1 5d\pi_u^2$, which results in a $^{19}\Sigma_g^-$ ground electronic state.

Spectroscopic data for Gd_2 were obtained in 2000 by Lombardi and co-workers via Raman and absorption spectroscopy in Ar matrices.[92] In this study, the ground state vibrational constant ω_e was measured to be 138.7 ± 0.4 cm^{-1}, and from this, along with the anharmonicity $\chi_e\omega_e$, the dissociation energy was determined to be 2.1 ± 0.7 eV. This value, however, differs significantly from the thermochemically determined dissociation energy of 1.784 ± 0.35 eV.[93] Other experimental studies have explored gadolinium in a variety of different environments to observe its magnetic properties. Schuh and co-workers measured the magnetic anisotropy energy (MAE) of gadolinium atoms and dimers on platinum and copper surfaces, finding possible application to quantum bit assembly due to the quantum nature of the spins in the localized $4f$ states.[94] Chang and co-workers synthesized Gd_{24} nanocapsules and observed an entropy change of 46.12 J kg^{-1} K^{-1}, making it a promising candidate as a molecular magnetic cryogenic material.[95] Gadolinium has also been studied in different manganese clusters which exhibited SMM behavior.[96,97]

A peculiarity that arises for the gadolinium dimer occurs upon dissociation into separate atoms (illustrated in Figure 4.2). The electronic configuration shows that, when bonded, three electrons exist within each of the *s* and *d* manifolds. However, for two noninteracting atoms, the electronic distribution changes. Instead, four electrons are contained in the *s* manifold, and only two electrons occupy the *d* manifold.

$(6s\sigma_g^2 6s\sigma_u^1 5d\sigma_g^1 5d\pi_u^2)$ $(6s^2 5d^1)$ $(6s^2 5d^1)$

Figure 4.2. Dissociation of Gd_2 to ground state atoms. The change in the valence electron configuration upon dissociation indicates an avoided crossing.

This circumstance confirms the presence of an avoided crossing upon dissociation, and also implies the existence of numerous low-lying excited states. For multiple states that are energetically proximate, mixing among atomic states with different *5d* and/or *4f* occupancy may occur, indicating that electron correlation is a sensitive property in this system and must be treated carefully in theoretical considerations.

Computational Details

A model space was constructed by partitioning the molecular orbitals into eight orbital groups, using a macroconfiguration method, which imposes restrictions on group occupancy. Within each orbital group, all possible electronic configurations subject to the given symmetry and multiplicity restrictions are allowed. The Gd_2 molecule was

55

considered in D_{2h} in order to make use of Abelian point group symmetry, and additional specialized angular momentum based routines ensured $D_{\infty h}$ symmetry. The 46 orbitals corresponding to the $1s$-$4d$ shells were considered in the core and remained doubly occupied throughout the calculations. At the MCSCF level, the $5s$ and $5p$ shells were also placed in the core to remain doubly occupied; however, at higher levels of correlation, i.e., the GVVPT2 level, these orbitals were placed in an active core group with single and double excitations allowed to the active orbital groups. The $4f$ orbitals were grouped based on the nature of the orbital, i.e., four different orbital groups for the $4f$ orbitals ($4f\sigma$, $4f\pi$, $4f\delta$, $4f\varphi$) were generated as part of the active space. The $6s\sigma$ and $5d\sigma$ orbitals were placed in one active orbital group, while the $5d\pi$ orbitals were placed in a separate active orbital group. This orbital partitioning scheme is presented in more detail in Table 4.1.

Table 4.1. Details of the active space used to describe Gd_2.

Orbital Group	a_g	b_{1g}	b_{2g}	b_{3g}	a_u	b_{1u}	b_{2u}	b_{3u}
$G_{Frozen\ Core}$	11	2	5	5	2	11	5	5
$G_{Active\ Core}$	2	0	1	1	0	2	1	1
$G_{4f\sigma}$	1	0	0	0	0	1	0	0
$G_{4f\pi}$	0	0	1	1	0	0	1	1
$G_{4f\delta}$	1	1	0	0	1	1	0	0
$G_{4f\varphi}$	0	0	1	1	0	0	1	1
$G_{(6s+5d)\sigma}$	2	0	0	0	0	2	0	0
$G_{5d\pi}$	0	0	1	1	0	0	1	1

For the ground state, a single reference macroconfiguration was used. The 14 electrons within the f shell were distributed so as to remain ferromagnetically coupled. The six valence electrons were distributed among the valence orbital groups so as to reflect the ground state electronic configuration, viz.,

$$\kappa_0^{Gd}(N) = (4f\sigma)^2(4f\pi)^4(4f\delta)^4(4f\varphi)^4\big((6s+5d)\sigma\big)^4(5d\pi)^2.$$

By imposing the spin restriction to ensure 19-plet multiplicity, the electron distribution within the $G_{(6s+5d)\sigma}$ orbital group breaks down as $((6s+5s)\sigma)^4 \rightarrow (6s\sigma_g)^2(6s\sigma_u)^1(5d\sigma_g)^1$, in agreement with the ground state electronic configuration.

Beyond the ground state, low-lying 19-plet and 17-plet excited states corresponding to various electronic transitions to and/or from the σ manifold were also considered in the study of Gd_2. Comparable to the ground state, a single macroconfiguration was used to describe the model space, with a similar treatment of the f electrons. The electronic states under consideration with their corresponding electronic transition are summarized in Table 4.2, while the macroconfigurations used to describe each of the states are given in Table 4.3.

Table 4.2. Electronic transitions and corresponding irreps and valence orbital configurations for the ground and excited states considered for Gd_2.

Transition	D_{2h} State	$D_{\infty h}$ State	Valence Orbital Configuration
Ground State	$^{19}B_{1g}$	$^{19}\Sigma_g^-$	$6s\sigma_g^2 6s\sigma_u^1 5d\sigma_g^1 5d\pi_u^2$
$\sigma \rightarrow \sigma^*$	$^{19}A_u$	$^{19}\Sigma_u^-$	$6s\sigma_g^1 6s\sigma_u^2 5d\sigma_g^1 5d\pi_u^2$
$\sigma \rightarrow \pi$	$^{19}B_{3u}$	$^{19}\Pi_u$	$6s\sigma_g^1 6s\sigma_u^1 5d\sigma_g^1 5d\pi_u^3$
$\sigma \rightarrow \delta$	$^{19}A_g$	$^{19}\Sigma_g^+$	$6s\sigma_g^1 6s\sigma_u^1 5d\sigma_g^1 5d\pi_u^2 5d\delta^1$
$\sigma^* \rightarrow \sigma$	$^{17}A_u$	$^{17}\Sigma_u^-$	$6s\sigma_g^2 6s\sigma_u^0 5d\sigma_g^2 5d\pi_u^2$
$\pi \rightarrow \sigma^*$	$^{17}B_{2g}$	$^{17}\Pi_g$	$6s\sigma_g^2 6s\sigma_u^2 5d\sigma_g^1 5d\pi_u^1$
$\pi \rightarrow \sigma$	$^{17}B_{3u}$	$^{17}\Pi_u$	$6s\sigma_g^2 6s\sigma_u^1 5d\sigma_g^2 5d\pi_u^1$

Table 4.3. Macroconfigurations for each electronic state used for the GVVPT2 calculations of Gd_2.

State	Macroconfiguration
$^{19}\Sigma_g^-$	$\kappa_0^{Gd}(N) = (4f\sigma)^2 (4f\pi)^4 (4f\delta)^4 (4f\varphi)^4 \left((6s+5d)\sigma\right)^4 (5d\pi)^2$
$^{19}\Sigma_u^-$	$\kappa_1^{Gd}(N) = (4f\sigma)^2 (4f\pi)^4 (4f\delta)^4 (4f\varphi)^4 \left((6s+5d)\sigma\right)^4 (5d\pi)^2$
$^{19}\Pi_u$	$\kappa_2^{Gd}(N) = (4f\sigma)^2 (4f\pi)^4 (4f\delta)^4 (4f\varphi)^4 \left((6s+5d)\sigma\right)^3 (5d\pi)^3$
$^{19}\Sigma_g^+$	$\kappa_3^{Gd}(N) = (4f\sigma)^2 (4f\pi)^4 (4f\delta)^4 (4f\varphi)^4 \left((6s+5d)\sigma\right)^3 (5d\pi)^2 (5d\delta)^1$
$^{17}\Sigma_u^-$	$\kappa_4^{Gd}(N) = (4f\sigma)^2 (4f\pi)^4 (4f\delta)^4 (4f\varphi)^4 \left((6s+5d)\sigma\right)^4 (5d\pi)^2$
$^{17}\Pi_g$	$\kappa_5^{Gd}(N) = (4f\sigma)^2 (4f\pi)^4 (4f\delta)^4 (4f\varphi)^4 \left((6s+5d)\sigma\right)^5 (5d\pi)^1$
$^{17}\Pi_u$	$\kappa_6^{Gd}(N) = (4f\sigma)^2 (4f\pi)^4 (4f\delta)^4 (4f\varphi)^4 \left((6s+5d)\sigma\right)^5 (5d\pi)^1$

Potential energy curves for the electronic states of Gd_2 described above were

constructed using GVVPT2 from MCSCF wavefunctions within the UNDMOL electronic

structure software package. The GVVPT2 method is known to provide a very accurate

treatment of electron correlation among a variety of chemical systems, including transition metal dimers recently characterized by Tamukong et al., which provides impetus for GVVPT2 to produce accurate descriptions for lanthanide dimer systems as well. Scalar relativistic effects were included through the use of the spin-free X2C Hamiltonian. The basis set employed to perform these calculations was an ANO-type VTZ basis set, consisting of a (25s22p15d11f4g) primitive set contracted to [8s7p4d3f2g]. The system was considered within the D_{2h} point group in order to make use of Abelian point group symmetry. Additional specialized angular momentum based routines ensured that $D_{\infty h}$ symmetry was preserved.

Results

The potential energy curves obtained for the ground and low-lying 19-plet excited states ($X^{19}\Sigma_g^-$, $1^{19}\Sigma_u^-$, $1^{19}\Sigma_g^+$) of Gd_2 from the scalar relativistic GVVPT2 calculations are shown in Figure 4.3. The leading configuration contributing to the ground electronic state wavefunction was found to be $(4f^7)(4f^7)6s\sigma_g^2 6s\sigma_u^1 5d\sigma_g^1 5d\pi_u^2$ with a weight of 0.96 at the calculated minimum. This predicts the ground state to be $^{19}B_{1g}$ in D_{2h} symmetry, which corresponds to $^{19}\Sigma_g^-$ in $D_{\infty h}$ symmetry, in agreement with previous experimental and theoretical results.
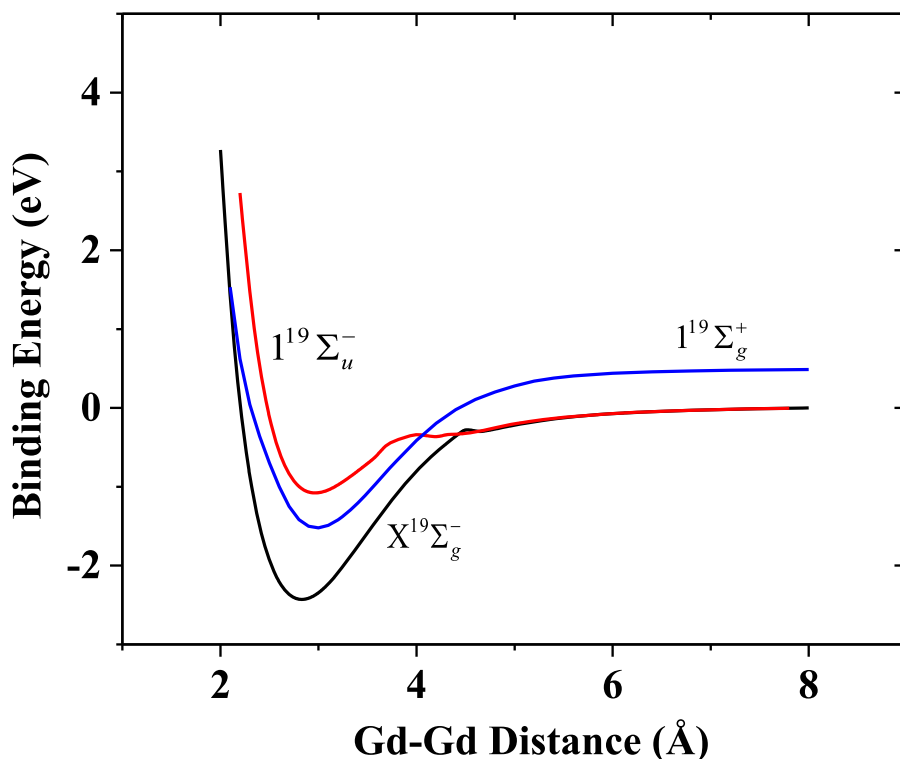
Figure 4.3. Potential energy curves for the ground and low-lying 19-plet excited states, $X^{19}\Sigma_g^-$, $1^{19}\Sigma_u^-$, $1^{19}\Sigma_g^+$, of Gd_2 obtained at the GVVPT2 level of theory.

The corresponding spectroscopic constants characterizing the curves in Figure 4.3 are displayed in Table 4.4. The equilibrium bond length for the ground state determined from these calculations is only slightly shorter than those obtained in previous theoretical studies (2.826 Å vs. 2.877 Å). The vibrational frequency obtained ($\omega_e = 153$ cm^{-1}) is also in reasonable agreement with the values obtained from other theoretical ($\omega_e = 149 \pm 2$ cm^{-1}) and experimental ($\omega_e = 138.7 \pm 0.4$ cm^{-1}) work. While the dissociation energy differs

largely from the CCSD(T) results (2.48 eV vs. 1.60 ± 0.18 eV), it is well within the error bars of the experimentally determined energy (2.1 ± 0.7 eV). Upon inclusion of spin-orbit coupling, it is expected that these results will coalesce with the experimental values.[71] This implies that the model chosen for Gd_2 is accurate, and also that GVVPT2 characterizes this system exceptionally well.

Table 4.4. Equilibrium distances (R_e), binding energies (D_e), and vibrational frequencies (ω_e) for the ground and low-lying 19-plet and 17-plet excited states of Gd_2 calculated at the GVVPT2 level of theory.

State	R_e (Å)	D_e (eV)	ω_e (cm⁻¹)
$^{19}\Sigma_g^-$	2.826	2.48	153.0
$^{19}\Sigma_g^+$	2.983	2.01	136.7
$^{19}\Sigma_u^-$	2.959	1.08	132.5
$^{17}\Sigma_u^-$	2.841	1.96	153.8
$^{17}\Pi_g$	3.251	0.90	107.4

Upon dissociation, the $^{19}\Sigma_g^-$ curve experiences a small hump around 4.5 Å. This is where the avoided crossing with an excited state is expected to take place. As Gd_2 dissociates, the valence electron configuration changes. The shape of the ground state curve obtained from the GVVPT2 calculations reflects that change.

The $^{19}\Sigma_u^-$ curve also exhibits small variations in energy within the range of 3.5-4.5 Å. Since the gadolinium atom has several accessible energy levels within a small energy range, many low-lying excited states may exist. It is expected that these changes in the

potential energy curve are due to close approaches or avoided crossings with other low-lying excited states.

The $^{19}\Sigma_g^+$ and $^{19}\Sigma_u^-$ states are more weakly bound and have a broader minimum than the $^{19}\Sigma_g^-$ state ($^{19}\Sigma_g^+$: $D_e = 2.01$ eV, $\omega_e = 136.7$ cm^{-1}; $^{19}\Sigma_u^-$: $D_e = 1.08$ eV, $\omega_e = 132.5$ cm^{-1}). The equilibrium bond length for these states is slightly longer than the ground state ($R_e = 2.983$ Å for $^{19}\Sigma_g^+$, $R_e = 2.959$ Å for $^{19}\Sigma_u^-$). This is due to a possible decrease in the bond order since these excited states promote an electron out of the $6s\sigma_g$ bonding orbital to anti-bonding orbitals. The potential energy curve for the $^{19}\Sigma_u^-$ state correlates with the same dissociation limit as the ground state. However, the curve for the $^{19}\Sigma_g^+$ state dissociates to a limit that is 0.49 eV higher in energy than the ground state. This behavior is expected as the $^{19}\Sigma_u^-$ state corresponds to an electronic transition of $\sigma \rightarrow \sigma^*$, meaning that the number of electrons in the respective s and d manifolds does not change relative to the ground state. The $^{19}\Sigma_g^+$ state corresponds to an electronic transition of $\sigma \rightarrow \delta$, requiring one of the s electrons to be promoted to the d manifold. Therefore, the dissociated atoms are expected to be at a higher energy than the ground state, and this is reflected in the GVVPT2 results.

62
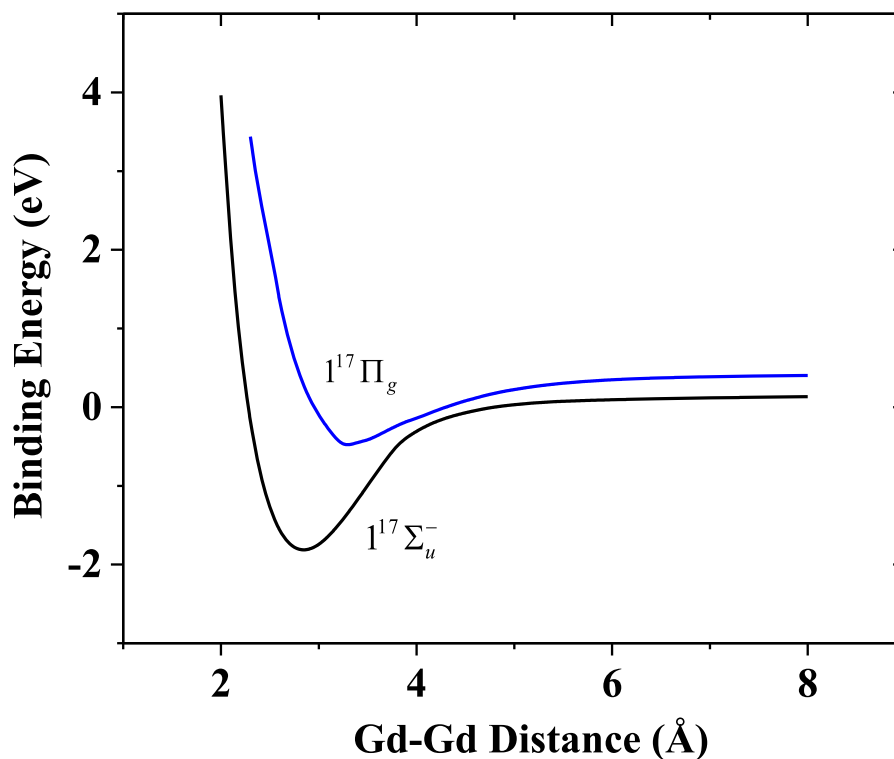
Figure 4.4. Potential energy curves for the low-lying 17-plet excited states, $1^{17}\Sigma_u^-$, $1^{17}\Pi_g$, of Gd_2 obtained at the GVVPT2 level of theory.

Similar to the 19-plet excited states, the $^{17}\Sigma_u^-$ and $^{17}\Pi_g$ states (Figure 4.4) are more weakly bonded compared to the ground state ($^{17}\Sigma_u^-$: D_e = 1.96 eV, $^{17}\Pi_g$: D_e = 0.90 eV). While the potential well is much broader for the $^{17}\Pi_g$ state (ω_e = 107.4 cm^{-1}), the vibrational frequency for the $^{17}\Sigma_u^-$ state (ω_e = 153.8 cm^{-1}) is comparable to the ground state. The equilibrium bond length for the $^{17}\Sigma_u^-$ state (R_e = 2.841 Å) is also very similar to the ground state, which coincides with the corresponding type of electronic transition ($\sigma^* \rightarrow$

σ). The $^{17}\Pi_g$ state shows a significant increase in bond length (R_e = 3.251 Å). Since, for this state, population of the $6s\sigma_u^*$ anti-bonding orbital is increased attributable to the associated electron transition, bond order obviously decreases and bond length increases. The dissociation limits for these states both lie within 0.5 eV of the ground state. As the gadolinium atom is known to have a large number of easily accessible energy levels, it follows that the dimer will have a significant number of low-lying excited states, as is observed from the results of the GVVPT2 calculations.

These results represent the first full potential energy curves generated for the ground and low-lying excited states of Gd_2. Although these calculations only include scalar relativistic effects, the close agreement achieved by these calculations for the ground state with experimental data further demonstrates the applicability of the GVVPT2 method to metal dimer systems. It also shows that the model space presented in this work is sufficient in describing ground and low-lying excited states of Gd_2, incentivizing GVVPT2 studies on other f-block metal dimer systems (such as Dy_2 presented in Chapter 5). Potential energy curves for other excited states corresponding to electronic transitions to and from the π manifold (i.e., $^{19}\Pi_u$ and $^{17}\Pi_u$) are currently being constructed. Calculations including spin-orbit relativistic effects at the GVVPT2 level on these systems need to be performed in order to obtain a more complete understanding of them.

CHAPTER V

RELATIVISTIC GVVPT2 STUDY OF GROUND AND LOW-LYING EXCITED

STATES OF THE DYSPROSIUM DIMER

Introduction

Among some of the other lanthanides receiving considerable attention as SMM

cores is dysprosium. In its ground state, the dysprosium atom has a ground electronic

configuration of $[Xe]4f^{10}6s^2$ (shown in Figure 5.1).[98] With four unpaired electrons all in

the f shell, the ground state has an atomic term symbol of $^5I_8$, giving dysprosium one of the

highest angular momentum values of any atom ($l = 6$) in its ground state.

Figure 5.1. Valence electron configuration of the Dysprosium atom.

It also exhibits a very large effective magnetic moment ($\mu_B^{eff} \approx 10.5$), which, along with

its relatively high ground state spin multiplicity, makes it a good candidate to be used in

SMMs.

A 2006 study by Powell et al. synthesized oxo-bridged dysprosium triangles and

showed that although the ground state is nearly non-magnetic, the thermally populated

excited states exhibit SMM behavior with a slow relaxation of the magnetization.[99] In

2013, Zheng et al. studied the magnetic properties of a hydrated and dehydrated oxo-

bridged dinuclear dysprosium complex.[100] The results showed that the dehydrated

complex had an enhanced magnetic anisotropy over the hydrated complex, and that the

relaxation processes were extremely sensitive to the degree of dehydration, allowing a reversible change of the magnetic properties through desorption and absorption cycles of solvent water. This outcome suggests that responsive functional materials based on lanthanide complexes could be designed. A comparative study of different homodinuclear lanthanide complexes (Gd, Tb, Dy, and Eu) was performed by Chandrasekhar et al. in 2015.[101] Of the complexes studied, the Dy-based complex showed the greatest SMM behavior with a two-step relaxation of magnetization process, indicated by the presence of two distinct peaks appearing in alternating current susceptibility measurements. After Arrhenius analysis, effective energy barriers of $U_{eff} = 8.96$ K and 35.5 K were found with respective pre-exponential factors of $\tau_0 = 8.81 \times 10^{-5}$ s and 1.48×10^{-6} s (when fit to the Arrhenius expression $\tau = \tau_0 \exp(U_{eff}/kT)$), corresponding to the fast and slow relaxations, respectively. By examining the relationship between the natural logarithm of the relaxation times with the inverse temperature, proportionality was observed for temperatures above 4.5 K, but a weaker dependency was observed for temperatures below 4.5 K. This behavior is characteristic of a crossover from a thermally activated Orbach mechanism above this temperature to a quantum tunneling process for the lower temperatures. Further analysis of this data using a generalized Debye model and Cole-Cole plots found a broader distribution of obtained α values in the range of 2-5.2 K, supporting the theory of two relaxation processes in operation in this range. A more narrow distribution was found at temperatures above 5.6 K, suggesting that the relaxation at higher

66

temperatures is dominated by a Raman process. The results also revealed a large discrepancy between the theoretical (20 μ_B) and experimental (11.5 μ_B) magnetization values at 7 T, which implies a significant magnetic anisotropy and/or the presence of low-lying excited states that are partially populated. Direct-current magnetic susceptibility studies supported this claim. At room temperature, the χT value was measured as 29.2 cm^3 K mol^{-1} and decreased gradually with temperature down to 40 K. Below this temperature, however, the χT value falls abruptly to 5.0 cm^3 K mol^{-1} at 2 K. This indicates progressive depopulation of excited Stark sublevels generated by the ligand field. Similar behavior, which is characteristic of SMMs, was observed in several other Dy-based complexes.[102–106]

Although these complexes mainly consist of bridged dysprosium cores, it would be apposite to investigate a directly bonded Dy$_2$ species, as the properties of this system remain unexplored. As a dimer, the electrons within the $6s$ atomic orbitals redistribute among the molecular orbitals, with one electron moving into the π (or δ) manifold, as shown in Figure 5.2.
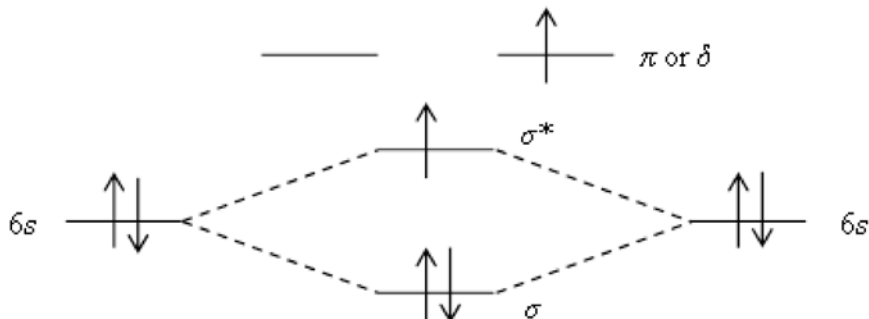
Figure 5.2. Valence orbital diagram for Dy$_2$. The higher energy molecular π (or δ) orbital is possibly generated by empty $5d$ atomic orbitals.

The f subvalence shell corresponds to a totally symmetric nonet substate. Therefore, it is expected that the ground state of this molecule will be $^{11}\Pi_g$. Nonet excited states could arise from this ground state from either an electron pairing ($^9\Sigma_g^+$) or spin-flip ($^9\Pi_g$) process. Generation of a 13-plet excited state would require an excitation from the bonding σ orbital to the empty π (or δ) orbital and result in a $^{13}\Sigma_g^-$ state. However, this excitation is much higher in energy and will not be considered in this investigation.

Computational Details

A model space was constructed for the X $^{11}\Pi_g$ state by partitioning the molecular orbitals into separate orbital groups, also using a macroconfiguration method. Similar to the Gd$_2$ molecule, Dy$_2$ was considered in D_{2h} in order to make use of Abelian point group symmetry, with additional specialized angular momentum based routines to ensure $D_{\infty h}$ symmetry. At the MCSCF level, the 54 orbitals corresponding to the $1s$-$4d$ along with the $5s$ and $5p$ shells and a single bonding σ orbital were considered in the core and remained doubly occupied. The $4f$ shell was separated according to double and single occupation.

68

Therefore, the doubly occupied 4*f* orbital group consisted of six orbitals, while the singly occupied 4*f* orbital group consisted of eight orbitals. The last orbital group contained the antibonding σ^* orbital and a single bonding π (or δ) orbital. Single and double electron excitations were considered between the 4*f* orbital groups to allow for sufficient correlation within the *f* shell. This model space was used to generate an optimized set of orbitals for use at higher levels of correlation, i.e., GVVPT2.

In order to accurately characterize this system, correlation of the 5*s* and 5*p* shells is necessary. Therefore, at the GVVPT2 level, the 8 orbitals corresponding to the 5*s* and 5*p* shells were included in the calculations as a valence group rather than in the core. By treating the other valence orbitals similar to the MCSCF organization, this model space would be sufficient in providing an accurate description of Dy_2. However, due to the large degeneracy within the *f* shell with this level of correlation, the number of CSFs generated by each macroconfiguration exceeds the number of the variables that can be used within the calculation. Consequently, the active space must be broken down in order to reduce the number of CSFs. The orbital group containing the 5*s* and 5*p* orbitals was separated into two orbital groups based on the character of the molecular orbital (σ vs. π). The orbital group containing the doubly occupied 4*f* orbitals was treated similarly. This active space sufficiently reduced the number of CSFs generated by each macroconfiguration so that the calculations completed smoothly. A summary of the MCSCF and GVVPT2 active spaces used are provided in Tables 5.1 and 5.2, respectively.

69

Table 5.1. Details of the MCSCF active space used to generate optimized orbitals for Dy_2.

Orbital Group	a_g	b_{1g}	b_{2g}	b_{3g}	a_u	b_{1u}	b_{2u}	b_{3u}
$G_{Frozen\ Core}$	14	2	6	6	2	13	6	6
$G_{4f\ double}$	2	0	1	0	0	2	0	1
$G_{4f\ single}$	0	1	1	2	1	0	2	1
$G_{bonding}$	0	0	0	0	0	1	0	1

Table 5.2. Details of the GVVPT2 active space used for the X $^{11}\Pi_g$ state of Dy_2.

Orbital Group	a_g	b_{1g}	b_{2g}	b_{3g}	a_u	b_{1u}	b_{2u}	b_{3u}
$G_{Frozen\ Core}$	12	2	5	5	2	11	5	5
$G_{Soft\ Core\ \sigma}$	2	0	0	0	0	2	0	0
$G_{Soft\ Core\ \pi}$	0	0	1	1	0	0	1	1
$G_{4f\sigma\ double}$	2	0	0	0	0	2	0	0
$G_{4f\pi\ double}$	0	0	1	0	0	0	0	1
$G_{4f\ single}$	0	1	1	2	1	0	2	1
$G_{bonding}$	0	0	0	0	0	1	0	1

The $^{11}\Pi_g$ valence electronic configuration is expected to be $(6s\sigma_g)^2(6s\sigma_u)^1(5d\pi_g)^1$, with the 8 electrons within the singly occupied $4f$ orbital group and the 2 unpaired valence electrons being ferromagnetically coupled. This corresponds to an electron distribution (and reference macroconfiguration) of

$$\kappa_{0,0}^{MCSCF}(N) = \left(G_{4f\ dbl}\right)^{12}\left(G_{4f\ sngl}\right)^{8}(G_{bnd})^{2}$$

at the MCSCF level, and

$$\kappa_{0,0}^{GVVPT}(N) = (G_{SC\ \sigma})^8(G_{SC\ \pi})^8\left(G_{4f\sigma\ dbl}\right)^8\left(G_{4f\pi\ dbl}\right)^4\left(G_{4f\ sngl}\right)^8(G_{bnd})^2$$

at the GVVPT2 level. The other macroconfigurations used in the calculations were generated from single and double electron excitation within the *f* shell from the reference macroconfiguration. The macroconfigurations used to describe the ground state at the MCSCF and GVVPT2 levels are given in Table 5.3.

Table 5.3. Macroconfigurations used for the MCSCF and GVVPT2 calculations of the X $^{11}\Pi_g$ state of Dy_2.

Method	Macroconfiguration
MCSCF	$\kappa_{0,0}^{MCSCF}(\boldsymbol{N}) = \left(G_{4f\ \text{dbl}}\right)^{12}\left(G_{4f\ \text{sngl}}\right)^{8}\left(G_{\text{bnd}}\right)^{2}$
	$\kappa_{1,0}^{MCSCF}(\boldsymbol{N}) = \left(G_{4f\ \text{dbl}}\right)^{11}\left(G_{4f\ \text{sngl}}\right)^{9}\left(G_{\text{bnd}}\right)^{2}$
	$\kappa_{2,0}^{MCSCF}(\boldsymbol{N}) = \left(G_{4f\ \text{dbl}}\right)^{10}\left(G_{4f\ \text{sngl}}\right)^{10}\left(G_{\text{bnd}}\right)^{2}$
GVVPT2	$\kappa_{0,0}^{GVVPT}(\boldsymbol{N}) = (G_{SC\ \sigma})^{8}(G_{SC\ \pi})^{8}\left(G_{4f\sigma\ \text{dbl}}\right)^{8}\left(G_{4f\pi\ \text{dbl}}\right)^{4}\left(G_{4f\ \text{sngl}}\right)^{8}\left(G_{\text{bnd}}\right)^{2}$
	$\kappa_{1,0}^{GVVPT}(\boldsymbol{N}) = (G_{SC\ \sigma})^{8}(G_{SC\ \pi})^{8}\left(G_{4f\sigma\ \text{dbl}}\right)^{8}\left(G_{4f\pi\ \text{dbl}}\right)^{3}\left(G_{4f\ \text{sngl}}\right)^{9}\left(G_{\text{bnd}}\right)^{2}$
	$\kappa_{2,0}^{GVVPT}(\boldsymbol{N}) = (G_{SC\ \sigma})^{8}(G_{SC\ \pi})^{8}\left(G_{4f\sigma\ \text{dbl}}\right)^{7}\left(G_{4f\pi\ \text{dbl}}\right)^{4}\left(G_{4f\ \text{sngl}}\right)^{9}\left(G_{\text{bnd}}\right)^{2}$
	$\kappa_{3,0}^{GVVPT}(\boldsymbol{N}) = (G_{SC\ \sigma})^{8}(G_{SC\ \pi})^{8}\left(G_{4f\sigma\ \text{dbl}}\right)^{8}\left(G_{4f\pi\ \text{dbl}}\right)^{2}\left(G_{4f\ \text{sngl}}\right)^{10}\left(G_{\text{bnd}}\right)^{2}$
	$\kappa_{4,0}^{GVVPT}(\boldsymbol{N}) = (G_{SC\ \sigma})^{8}(G_{SC\ \pi})^{8}\left(G_{4f\sigma\ \text{dbl}}\right)^{7}\left(G_{4f\pi\ \text{dbl}}\right)^{3}\left(G_{4f\ \text{sngl}}\right)^{10}\left(G_{\text{bnd}}\right)^{2}$
	$\kappa_{5,0}^{GVVPT}(\boldsymbol{N}) = (G_{SC\ \sigma})^{8}(G_{SC\ \pi})^{8}\left(G_{4f\sigma\ \text{dbl}}\right)^{6}\left(G_{4f\pi\ \text{dbl}}\right)^{4}\left(G_{4f\ \text{sngl}}\right)^{8}\left(G_{\text{bnd}}\right)^{2}$

Similar to Gd_2, GVVPT2 calculations on the ground state of Dy_2 were performed using MCSCF reference wavefunctions within the UNDMOL electronic structure software package. The basis set employed throughout the calculations was an ANO-type TZP basis set, consisting of a (25s22p15d11f4g2h) primitive set contracted to [8s7p4d3f2g1h].[107] Scalar relativistic effects were included through the use of the spin-free X2C Hamiltonian. The system was considered within the D_{2h} point group in order to make use of Abelian

point group symmetry, with additional specialized angular momentum based routines that ensured the preservation of $D_{\infty h}$ symmetry.

Since this scheme is sufficient in producing potential energy curves for the X $^{11}\Pi_g$ state of Dy_2, a similar treatment would be expected to successfully characterize the $^9\Sigma_g^+$ and $^9\Pi_g$ excited states. However, the reduction in multiplicity of this system allows for the generation of many more CSFs within the previously defined macroconfigurations, and results in exceeding the variable range. Therefore, a different construction of the model space is required for the nonet excited states.

Scalar relativistic potential energy curves for the X $^{11}\Pi_g$ state of Dy_2 will be generated at the GVVPT2 level. Upon determination of a suitable model space for the nonet excited states, potential energy curves will be produced for these states using GVVPT2 as well. Spin-orbit effects will be included in future considerations.

CHAPTER VI

FUTURE WORK: GVVPT2 STUDY OF THE SCANDIUM TRIMER

Although the previous two chapters focused on dimeric species, metallic trimers also provide a difficult yet interesting challenge, which also have their place in materials science applications.[108–118] The scandium atom has a ground state electronic configuration of $[Ar]3d^14s^2$ (shown in Figure 6.1).[119] While this element may seem to have a rather trivial configuration, the electronic structure becomes much more complicated when considering molecules formed with scandium atoms due to the degeneracy and accessibility of the $3d$ orbitals.[120]

Figure 6.1. Valence electron configuration of the Scandium atom.

Upon formation of a trimer, a rather interesting property arises. Considering that if the lone unpaired electron for each of these atoms remains localized to their respective atomic sites, two cases may arise: (i) the spin of the electrons remain aligned, forming a spin-coupled quartet, or (ii) one of the electrons will have a spin opposite of the other two, forming a spin frustrated doublet. An active area of research within condensed matter physics focuses on these spin frustrated systems.[121–134] Therefore, a theoretical understanding of Sc_3 will not only provide a base model for considering other metallic trimer systems, but also deliver supplementary information on spin frustrated systems.

The scandium trimer has been previously studied both experimentally and theoretically. In 1983 using ESR spectroscopy, Knight et al.[135] found that Sc_3 exists as an equilateral triangle, the lone unpaired electron being delocalized in the $3d$ orbitals among the Sc atoms, with a ground electronic state of $^2A_1'$. A year later, Moskovits et al.[136] reported a ground electronic state of $^2E'$ using resonance Raman spectroscopy for Sc_3, having what the authors describe as an equilateral or near equilateral triangular structure. The vibrational frequencies found in that study were 246 cm^{-1} for the symmetric stretch (ω_1), 151 cm^{-1} for the asymmetric stretch (ω_2), and 145 cm^{-1} for the bending mode (ω_3). A CASSCF/CCI study was conducted in 1985 by Walch and Bauschlicher[137] in an attempt to resolve this discrepancy. The results of that study showed the ground electronic state to be $^2A_2''$ with a Sc-Sc bond length of 3.04 Å. The authors also report that Sc_3 is rather strongly bound with a well depth of 1.0 eV. In 1997, Pápai and Castro[138] performed DFT calculations on Sc_3 and found a ground electronic state of $^2A_1'$, with the $^2A_2''$ and $^2E'$ states lying about 0.2 eV higher in energy. The equilibrium structures for the $^2A_1'$ and $^2A_2''$ states were determined to have D_{3h} symmetry, while the $^2E'$ state was determined to undergo a Jahn-Teller distortion and have an apex angle of 57.1°. The spectroscopic data presented in that study were in relative agreement with previous experimental data ($R_{Sc\text{-}Sc}$ = 2.83 Å, ω_1 = 272 cm^{-1}, ω_2 = 153 cm^{-1}, ω_3 = 153 cm^{-1}). Bérces also performed DFT calculations on Sc_3 in 1997[139] and found a $^2A_1'$ ground state with D_{3h} symmetry. Although the bond length was in relative agreement with other literature values ($R_{Sc\text{-}Sc}$ = 2.81 Å), the vibrational

frequencies showed significant deviation (ω_1 = 292 cm^{-1}, ω_2 = 238 cm^{-1}, ω_3 = 238 cm^{-1}). Another DFT study by Wu et al. in 2004[117] found results contradictory to previous work, with a ground state reported to be a C_{2v} quartet (6.2° distortion) that was 0.26 eV more stable in energy than the lowest doublet (also with C_{2v} symmetry). In 2005, Papas and Schaefer conducted a DFT study on Sc$_3$.[118] The results of that study showed the ground electronic state to be $^2A_1{}'$ with a Sc-Sc bond length of 2.83 Å, in qualitative agreement with other DFT results. The vibrational frequencies (ω_1 = 267 cm^{-1}, ω_2 = 139 cm^{-1}, ω_3 = 140 cm^{-1}) were also in reasonable agreement with the experimental results found by Moskovits et al. Furthermore, seven other low-lying excited states were found to exist within 0.403 eV of the ground state, exhibiting the complexity of the system. Although several studies have been performed on Sc$_3$, there is no clear consensus among the results. Previous studies have also focused on the system having a single unpaired delocalized electron, so the nature of the spin frustrated system remains virtually unexplored.

Previous success by Tamukong et al. in characterizing transition metal dimers with the GVVPT2 method[77,140] suggests that similar success can be obtained for the trimers as well. The planned investigation into Sc$_3$ will aim to accomplish three main objectives. First, the GVVPT2 method will be used to generate potential energy curves for the dissociation Sc$_3$ → Sc$_2$ + Sc, as well as to supplement previous results on Sc$_3$. Second, the theoretical study will provide a model successful in describing Sc$_3$ that will serve as a prototype when constructing models for 4d or 4f metal trimers. Lastly, the accuracy of the

75

results will be analyzed to determine the practicality of perturbation theory on spin frustrated transition metal systems.

APPENDIX A

THE SPIN-ORBIT TERM

A derivation of the spin-orbit term is presented here following the procedure demonstrated by Desai.[6]

Consider the Dirac equation for a particle in the presence of a spherically symmetric potential $V(r)$ (as is the case for electrons near nuclei in atoms)

$$[E - \boldsymbol{\alpha} \cdot \boldsymbol{p} - \beta m - V(r)]\varphi(\boldsymbol{r}) = 0, \tag{A.1}$$

where E is the energy eigenvalue for the particle. The operator $\boldsymbol{p}$ is understood to be represented by $-i\boldsymbol{\nabla}$, and $\boldsymbol{\alpha}$ and β are given in standard representation. The term $\varphi(\boldsymbol{r})$ is a four-component column matrix represented by a large component φ_L and a small component φ_S. In block matrix form, equation (A.1) reads

$$\begin{pmatrix} E - m - V & -\boldsymbol{\sigma} \cdot \boldsymbol{p} \\ -\boldsymbol{\sigma} \cdot \boldsymbol{p} & E + m - V \end{pmatrix} \begin{pmatrix} \varphi_L \\ \varphi_S \end{pmatrix} = 0. \tag{A.2}$$

This matrix equation can be broken down into a series of equations given by

$$(E - m - V)\varphi_L - \boldsymbol{\sigma} \cdot \boldsymbol{p}\varphi_S = 0, \tag{A.3}$$

$$-\boldsymbol{\sigma} \cdot \boldsymbol{p}\varphi_L + (E + m - V)\varphi_S = 0. \tag{A.4}$$

Let $|V| \ll m$ and consider the nonrelativistic limit $E \approx m$, with the kinetic energy E_T being expressed as

$$E - m = E_T. \tag{A.5}$$

Then equation (A.3) becomes

$$(E_T - V)\varphi_L = \boldsymbol{\sigma} \cdot \boldsymbol{p}\varphi_S. \tag{A.6}$$

Since in the nonrelativistic limit both E_T and $V \ll m$, equation (A.4) can be rewritten as

$$(2m + E_T - V)\varphi_S = \boldsymbol{\sigma} \cdot \boldsymbol{p}\varphi_L. \tag{A.7}$$

The small component of $\varphi(\boldsymbol{r})$ can be expressed in terms of the large component from this equation

$$\varphi_S = \frac{\boldsymbol{\sigma} \cdot \boldsymbol{p}}{(2m + E_T - V)} \varphi_L \tag{A.8}$$

$$\approx \frac{1}{2m}\left(1 - \frac{E_T - V}{2m}\right)\boldsymbol{\sigma} \cdot \boldsymbol{p}\varphi_L \tag{A.9}$$

$$\approx \left[\frac{\boldsymbol{\sigma} \cdot \boldsymbol{p}}{2m} - \left(\frac{E_T - V}{4m^2}\right)\boldsymbol{\sigma} \cdot \boldsymbol{p}\right]\varphi_L. \tag{A.10}$$

Substituting this relation into equation (A.6) allows one to rewrite the equation as

$$(E_T - V)\varphi_L = \frac{\boldsymbol{\sigma} \cdot \boldsymbol{p}}{2m}\left[1 - \left(\frac{E_T - V}{2m}\right)\right]\boldsymbol{\sigma} \cdot \boldsymbol{p}\varphi_L \tag{A.11}$$

$$= \left[\frac{(\boldsymbol{\sigma} \cdot \boldsymbol{p})(\boldsymbol{\sigma} \cdot \boldsymbol{p})}{2m} - \frac{\boldsymbol{\sigma} \cdot \boldsymbol{p}E_T\boldsymbol{\sigma} \cdot \boldsymbol{p}}{4m^2} + \frac{\boldsymbol{\sigma} \cdot \boldsymbol{p}V\boldsymbol{\sigma} \cdot \boldsymbol{p}}{4m^2}\right]\varphi_L \tag{A.12}$$

$$= \left[\frac{\boldsymbol{p}^2}{2m} - \frac{\boldsymbol{p}^2}{4m^2}E_T + \frac{\boldsymbol{\sigma} \cdot \boldsymbol{p}V\boldsymbol{\sigma} \cdot \boldsymbol{p}}{4m^2}\right]\varphi_L. \tag{A.13}$$

In this derivation, $\varphi(\boldsymbol{r})$ is considered to be normalized, so

$$\int d^3r \, \varphi^\dagger(\boldsymbol{r})\varphi(\boldsymbol{r}) = 1. \tag{A.14}$$

The product within the integrand can be re-expressed as $\varphi^\dagger \varphi = |\varphi|^2 = |\varphi_L|^2 + |\varphi_S|^2$. By making the substitution according to equation (A.10), the normalization condition can be rewritten as

$$\int d^3r \left(|\varphi_L|^2 + \frac{\boldsymbol{p}^2}{4m^2} |\varphi_L|^2 \right) = 1, \tag{A.15}$$

or

$$\int d^3r \left(1 + \frac{\boldsymbol{p}^2}{4m^2} \right) |\varphi_L|^2 = 1, \tag{A.16}$$

where terms of order $\left(\frac{v}{c} \right)^4$ have been neglected (as will be done throughout the remainder of this derivation). Note that while excluding these terms is not necessarily practical, it is sufficient for the purposes of this derivation.

A new wavefunction ψ is defined to be

$$\psi = \sqrt{1 + \frac{\boldsymbol{p}^2}{4m^2}} \, \varphi_L, \tag{A.17}$$

which also meets the normalization condition. Considering a Taylor series expansion of the square root, the new wavefunction can be expressed as

$$\psi = \left(1 + \frac{\boldsymbol{p}^2}{8m^2} \right) \varphi_L. \tag{A.18}$$

Rewriting φ_L in terms of ψ, then

79

$$\varphi_L = \left(1 - \frac{\boldsymbol{p}^2}{8m^2}\right)\psi. \tag{A.19}$$

Rearranging equation (A.13) gives

$$E_T\left(1 + \frac{\boldsymbol{p}^2}{4m^2}\right)\varphi_L = \left[\frac{\boldsymbol{p}^2}{2m} + V + \frac{\boldsymbol{\sigma}\cdot\boldsymbol{p}V\boldsymbol{\sigma}\cdot\boldsymbol{p}}{4m^2}\right]\varphi_L. \tag{A.20}$$

By substituting the relationship for φ_L according to equation (A.19) into equation (A.20), an expression in terms of the new wavefunction ψ is obtained

$$E_T\left(1 + \frac{\boldsymbol{p}^2}{4m^2}\right)\left(1 - \frac{\boldsymbol{p}^2}{8m^2}\right)\psi = E_T\left(1 + \frac{\boldsymbol{p}^2}{8m^2}\right)\psi$$

$$= \left[\frac{\boldsymbol{p}^2}{2m} + V + \frac{\boldsymbol{\sigma}\cdot\boldsymbol{p}V\boldsymbol{\sigma}\cdot\boldsymbol{p}}{4m^2}\right]\left(1 - \frac{\boldsymbol{p}^2}{8m^2}\right)\psi. \tag{A.21}$$

Multiplication on the left by $\left(1 - \frac{\boldsymbol{p}^2}{8m^2}\right)$ is performed on both sides of equation (A.21) and then expanded through terms of order $\left(\frac{v}{c}\right)^2$

$$E_T\psi = \left(1 - \frac{\boldsymbol{p}^2}{8m^2}\right)\left[\frac{\boldsymbol{p}^2}{2m} + V + \frac{\boldsymbol{\sigma}\cdot\boldsymbol{p}V\boldsymbol{\sigma}\cdot\boldsymbol{p}}{4m^2}\right]\left(1 - \frac{\boldsymbol{p}^2}{8m^2}\right)\psi \tag{A.22}$$

$$= \left[\frac{\boldsymbol{p}^2}{2m} - \frac{\boldsymbol{p}^4}{8m^3} + V - \frac{1}{8m^2}(V\boldsymbol{p}^2 + \boldsymbol{p}^2V) + \frac{\boldsymbol{\sigma}\cdot\boldsymbol{p}V\boldsymbol{\sigma}\cdot\boldsymbol{p}}{4m^2}\right]\psi. \tag{A.23}$$

This takes the form of the eigenvalue equation $H\psi = E_T\psi$, where the Hamiltonian is given by

$$H = \frac{\boldsymbol{p}^2}{2m} - \frac{\boldsymbol{p}^4}{8m^3} + V - \frac{1}{8m^2}(V\boldsymbol{p}^2 + \boldsymbol{p}^2V) + \frac{\boldsymbol{\sigma}\cdot\boldsymbol{p}V\boldsymbol{\sigma}\cdot\boldsymbol{p}}{4m^2}. \tag{A.24}$$

This expression can be simplified by the relation $\boldsymbol{\sigma}\cdot\boldsymbol{p}V\boldsymbol{\sigma}\cdot\boldsymbol{p} = -i\boldsymbol{\sigma}\cdot(\boldsymbol{\nabla}V)\boldsymbol{\sigma}\cdot\boldsymbol{p} + V\boldsymbol{p}^2$

$$H = \frac{\boldsymbol{p}^2}{2m} - \frac{\boldsymbol{p}^4}{8m^3} + V - \frac{1}{8m^2}(\boldsymbol{p}^2 V - V\boldsymbol{p}^2) - \frac{i\boldsymbol{\sigma} \cdot (\boldsymbol{\nabla}V)\boldsymbol{\sigma} \cdot \boldsymbol{p}}{4m^2}. \qquad (A.25)$$

Also, since H operates on the wavefunction ψ, it can be shown by application of the product

rule that

$$(\boldsymbol{p}^2 V - V\boldsymbol{p}^2)\psi = -(\boldsymbol{\nabla}^2 V)\psi - 2\boldsymbol{\nabla}V \cdot (\boldsymbol{\nabla}\psi)$$

$$= -(\boldsymbol{\nabla}^2 V)\psi + 2i\boldsymbol{\nabla}V \cdot (\boldsymbol{p}\psi). \qquad (A.26)$$

Furthermore, the Dirac identity can be applied to show that

$$\boldsymbol{\sigma} \cdot (\boldsymbol{\nabla}V)\boldsymbol{\sigma} \cdot \boldsymbol{p} = \boldsymbol{\nabla}V \cdot \boldsymbol{p} + i\boldsymbol{\sigma} \cdot (\boldsymbol{\nabla}V \times \boldsymbol{p}). \qquad (A.27)$$

Therefore, the Hamiltonian can then be re-expressed as

$$H = \frac{\boldsymbol{p}^2}{2m} - \frac{\boldsymbol{p}^4}{8m^3} + V + \frac{1}{8m^2}\boldsymbol{\nabla}^2 V + \frac{\boldsymbol{\sigma} \cdot (\boldsymbol{\nabla}V \times \boldsymbol{p})}{4m^2}. \qquad (A.28)$$

The potential $V = V(r)$ is defined to be spherically symmetric, so the gradient of

the potential can be written as

$$\boldsymbol{\nabla}V = \boldsymbol{r}\frac{1}{r}\frac{dV}{dr}, \qquad (A.29)$$

so then

$$\boldsymbol{\sigma} \cdot (\boldsymbol{\nabla}V \times \boldsymbol{p}) = \frac{1}{r}\frac{dV}{dr}\boldsymbol{\sigma} \cdot (\boldsymbol{r} \times \boldsymbol{p}) \qquad (A.30)$$

$$= \frac{1}{r}\frac{dV}{dr}\boldsymbol{\sigma} \cdot \mathbf{L}, \qquad (A.31)$$

where $\mathbf{L}$ is the angular momentum operator. By making the substitution $\mathbf{S} = \frac{1}{2}\boldsymbol{\sigma}$ for the

spin-operator, the Hamiltonian can finally be expressed as

$$H = \frac{\boldsymbol{p}^2}{2m} - \frac{\boldsymbol{p}^4}{8m^3} + V + \frac{1}{8m^2}\boldsymbol{\nabla}^2 V + \frac{1}{2m^2 r}\frac{dV}{dr}\mathbf{L}\cdot\mathbf{S}. \tag{A.32}$$

The last term in this expression corresponds to the spin-orbit coupling commonly observed

for spherically symmetric potentials.

REFERENCES

(1)   Gauss, J. In *Modern Wavefunction Based Methods in Electronic Structure Theory Summer School*; Gelsenkirchen, Germany, 2016.

(2)   Saue, T. In *Modern Wavefunction Based Methods in Electronic Structure Theory Summer School*; Gelsenkirchen, Germany, 2016.

(3)   Liu, W. *Natl. Sci. Rev.* **2015**, *62* (1), 62–66.

(4)   Schwarz, W. H. E.; Wezenbeek, E. M. van; Baerends, E. J.; Snijders, J. G. *J. Phys. B At. Mol. Opt. Phys.* **1989**, *22* (10), 1515–1529.

(5)   Baerends, E.J.; Schwarz, W.H.E.; Schwerdtfeger, P.; Snijders, J. *J. Phys. B At. Mol. Phys.* **1990**, *23*, 3225–3240.

(6)   Desai, B. R. *Quantum Mechanics with Basic Field Theory*; Cambridge University Press: Cambridge, UK, 2010.

(7)   Yarkony, D. R. *Int. Rev. Phys. Chem.* **1992**, *11* (2), 195–242.

(8)   Fedorov, D. G.; Koseki, S.; Schmidt, M. W.; Gordon, M. S. *Int. Rev. Phys. Chem.* **2003**, *22* (3), 551–592.

(9)   Marian, C. M. *Wiley Interdiscip. Rev. Comput. Mol. Sci.* **2012**, *2* (2), 187–203.

(10)   Singleton, D. L.; Furuyama, S.; Cvetanović, R. J.; Irwin, R. S. *J. Chem. Phys.* **1975**, *63* (2), 1003–1007.

(11)   Dupuis, M.; Wendoloski, J. J.; Takada, T.; Lester, W. A. *J. Chem. Phys.* **1982**, *76* (1), 481–487.

(12)   Nguyen, T. L.; Vereecken, L.; Hou, X. J.; Nguyen, M. T.; Peeters, J. *J. Phys. Chem. A* **2005**, *109* (33), 7489–7499.

(13)   Nguyen, T. L.; Peeters, J.; Vereecken, L. *J. Phys. Chem. A* **2007**, *111* (19), 3836–3849.

(14)   Sabbah, H.; Biennier, L.; Sims, I. R.; Georgievskii, Y.; Klippenstein, S. J.; Smith, I. W. M. *Science (80-.).* **2007**, *317* (5834), 102–105.

(15)   Taatjes, C. A.; Osborn, D. L.; Selby, T. M.; Meloni, G.; Trevitt, A. J.; Epifanovsky, E.; Krylov, A. I.; Sirjean, B.; Dames, E.; Wang, H. *J. Phys. Chem. A* **2010**, *114* (9), 3355–3370.

(16)   Fu, B.; Han, Y.-C.; Bowman, J. M.; Leonori, F.; Balucani, N.; Angelucci, L.; Occhiogrosso, A.; Petrucci, R.; Casavecchia, P. *J. Chem. Phys.* **2012**, *137* (22), 22A532.

(17)   West, A. C.; Lynch, J. D.; Sellner, B.; Lischka, H.; Hase, W. L.; Windus, T. L. *Theor. Chem. Acc.* **2012**, *131* (10), 1279.

(18)   West, A. C.; Lynch, J. D.; Sellner, B.; Lischka, H.; Hase, W. L.; Windus, T. L. *Theor. Chem. Acc.* **2012**, *131* (3), 1123.

(19)   Ha, T.; Tinnefeld, P. *Annu. Rev. Phys. Chem.* **2012**, *63* (1), 595–617.

(20)   Sun, Y.; Giebink, N. C.; Kanno, H.; Ma, B.; Thompson, M. E.; Forrest, S. R. *Nature* **2006**, *440* (7086), 908–912.

(21)   Pyykko, P.; Desclaux, J. P. *Acc. Chem. Res.* **1979**, *12* (8), 276–281.

(22)   Silver, M. A.; Cary, S. K.; Johnson, J. A.; Baumbach, R. E.; Arico, A. A.; Luckey, M.; Urban, M.; Wang, J. C.; Polinski, M. J.; Chemey, A.; Liu, G.; Chen, K.-W.; Van Cleve, S. M.; Marsh, M. L.; Eaton, T. M.; van de Burgt, L. J.; Gray, A. L.; Hobart, D. E.; Hanson, K.; Maron, L.; Gendron, F.; Autschbach, J.; Speldrich, M.; Kogerler, P.; Yang, P.; Braley, J.; Albrecht-Schmitt, T. E. *Science (80-.)*. **2016**, *353* (6302), aaf3762-aaf3762.

(23)   Moreno, N.; Ferraro, F.; Flórez, E.; Hadad, C. Z.; Restrepo, A. *J. Phys. Chem. A* **2016**, *120* (10), 1698–1705.

(24)   Kovács, A. *J. Phys. Chem. A* **2017**, *121* (12), 2523–2530.

(25)   Singh, V.; Pulikkotil, J. J. *Phys. B Condens. Matter* **2017**, *519*, 59–62.

(26)   Cantero-López, P.; Páez-Hernández, D.; Arratia-Pérez, R. *Chem. Phys. Lett.* **2017**, *685*, 60–68.

(27)   Notter, F.-P.; Dubillard, S.; Bolvin, H. *J. Chem. Phys.* **2008**, *128* (16), 164315.

(28)   Pahl, E.; Figgen, D.; Thierfelder, C.; Peterson, K. A.; Calvo, F.; Schwerdtfeger, P. *J. Chem. Phys.* **2010**, *132* (11), 114301.

(29)   Pahl, E.; Figgen, D.; Borschevsky, A.; Peterson, K. A.; Schwerdtfeger, P. *Theor. Chem. Acc.* **2011**, *129* (3–5), 651–656.

(30)   Ferraro, F.; Arratia-Pérez, R. *Polyhedron* **2011**, *30* (5), 860–863.

(31)   Błoński, P.; Dennler, S.; Hafner, J. *J. Chem. Phys.* **2011**, *134* (3), 034107.

(32)   Tecmer, P.; van Lingen, H.; Gomes, A. S. P.; Visscher, L. *J. Chem. Phys.* **2012**,

137 (8), 084308.

(33)   Mishra, V.; Gyanchandani, J.; Chaturvedi, S.; Sikka, S. K. *Solid State Commun.* **2014**, *186*, 38–41.

(34)   Peterson, C.; Penchoff, D. A.; Wilson, A. K. *J. Chem. Phys.* **2015**, *143* (19), 194109.

(35)   Pyykkö, P. *Chem. Rev.* **1988**, *88* (3), 563–594.

(36)   Minaev, B. *Chem. Phys. Lett.* **1998**, *295* (5–6), 455–461.

(37)   Bagno, A.; Rastrelli, F.; Saielli, G. *J. Phys. Chem. A* **2003**, *107* (46), 9964–9973.

(38)   Visscher, L.; Dyall, K. G.; Lee, T. J. *Int. J. Quantum Chem.* **1995**, *56* (S29), 411–419.

(39)   Kelley, M. S.; Shiozaki, T. *J. Chem. Phys.* **2013**, *138* (20), 204113.

(40)   Liu, W. *Phys. Chem. Chem. Phys.* **2012**, *14* (1), 35–48.

(41)   Foldy, L. L.; Wouthuysen, S. A. *Phys. Rev.* **1950**, *78* (1), 29–36.

(42)   Douglas, M.; Kroll, N. M. *Ann. Phys. (N. Y).* **1974**, *82* (1), 89–155.

(43)   Chang, C.; Pelissier, M.; Durand, P. *Phys. Scr.* **1986**, *34* (5), 394–404.

(44)   Hess, B. A. *Phys. Rev. A* **1985**, *32* (2), 756–763.

(45)   Hess, B. A. *Phys. Rev. A* **1986**, *33* (6), 3742–3748.

(46)   Heully, J.-L.; Lindgren, I.; Lindroth, E.; Lundqvist, S.; Martensson-Pendrill, A.-M. *J. Phys. B At. Mol. Phys.* **1986**, *19* (18), 2799–2815.

(47)   Barysz, M.; Sadlej, A. J.; Snijders, J. G. *Int. J. Quantum Chem.* **1997**, *65* (3), 225–

239.

(48)   Nakajima, T.; Hirao, K. *Chem. Phys. Lett.* **1999**, *302* (5–6), 383–391.

(49)   Peng, D.; Reiher, M. *J. Chem. Phys.* **2012**, *136* (24), 244108.

(50)   Kutzelnigg, W.; Liu*, W. *Mol. Phys.* **2006**, *104* (13–14), 2225–2240.

(51)   Liu, W. *Mol. Phys.* **2010**, *108* (13), 1679–1706.

(52)   Heß, B. A.; Marian, C. M.; Wahlgren, U.; Gropen, O. *Chem. Phys. Lett.* **1996**, *251* (5–6), 365–371.

(53)   Parlant, G.; Rostas, J.; Taieb, G.; Yarkony, D. R. *J. Chem. Phys.* **1990**, *93* (9), 6403–6418.

(54)   Vahtras, O.; Ågren, H.; Jo/rgensen, P.; Jo/rgen Aa. Jensen, H.; Helgaker, T.; Olsen, J. *J. Chem. Phys.* **1992**, *96* (3), 2118–2126.

(55)   Mai, S.; Müller, T.; Plasser, F.; Marquetand, P.; Lischka, H.; González, L. *J. Chem. Phys.* **2014**, *141* (7), 074105.

(56)   Shiozaki, T.; Mizukami, W. *J. Chem. Theory Comput.* **2015**, *11* (10), 4733–4739.

(57)   Ghosh, A.; Chaudhuri, R. K.; Chattopadhyay, S. *J. Chem. Phys.* **2016**, *145* (12), 124303.

(58)   Visscher, L.; Lee, T. J.; Dyall, K. G. *J. Chem. Phys.* **1996**, *105* (19), 8769–8776.

(59)   Christiansen, O.; Gauss, J.; Schimmelpfennig, B. *Phys. Chem. Chem. Phys.* **2000**, *2* (5), 965–971.

(60)   Sur, C.; Chaudhuri, R. K. *Phys. Rev. A* **2007**, *76* (1), 012509.

(61)   Klein, K.; Gauss, J. *J. Chem. Phys.* **2008**, *129* (19), 194106.

(62)   Figgen, D.; Saue, T.; Schwerdtfeger, P. *J. Chem. Phys.* **2010**, *132* (23), 234310.

(63)   Mück, L. A.; Gauss, J. *J. Chem. Phys.* **2012**, *136* (11), 111103.

(64)   Komorovsky, S.; Repisky, M.; Ruud, K.; Malkina, O. L.; Malkin, V. G. *J. Phys. Chem. A* **2013**, *117* (51), 14209–14219.

(65)   Li, Z.; Suo, B.; Zhang, Y.; Xiao, Y.; Liu, W. *Mol. Phys.* **2013**, *111* (24), 3741–3755.

(66)   Li, Z.; Xiao, Y.; Liu, W. *J. Chem. Phys.* **2014**, *141* (5).

(67)   Martin, W.C.; Zalubas, Romuald; Hagan, L. *Atomic Energy Levels - The Rare Earth Elements*; National Bureau of Standards: Washington, D.C., 1978.

(68)   Stenbeck, G.; So, T. H.; James, E.; Young, S. W.; Qing, F.; Harriman, A.; Sessler, J. L.; Dow, W. C.; Mody, T. D.; Hemmi, W.; Hao, Y.; Miller, R. a; Wiles, K.; Hesselberth, J.; Liu, L.; Greenberg, E. P.; Valore, E. V; Michael, J.; Ganz, T.; Tack, B. F.; Mccray, P. B.; Doyle, A.; Yang, W.; Abruzzo, L. V; Gao, Y.; Rishi, A. K.; Douglas, D. *Proc. Natl. Acad. Sci. USA* **1996**, *93*, 6610–6615.

(69)   Van Zee, R. J.; Li, S.; Weltner, W. *J. Chem. Phys.* **1994**, *100* (5), 4010–4012.

(70)   Dolg, M.; Stoll, H.; Preuss, H. *J. Mol. Struct. THEOCHEM* **1992**, *277*, 239–249.

(71)   Dolg, M.; Liu, W.; Kalvoda, S. *Int. J. Quantum Chem.* **2000**, *76* (3), 359–370.

(72)   CAO, X.; DOLG, M. *Mol. Phys.* **2003**, *101* (13), 1967–1976.

(73)   Rinehart, J. D.; Long, J. R. *Chem. Sci.* **2011**, *2* (11), 2078.

(74)   Watson, A. D. *J. Alloys Compd.* **1994**, *207–208*, 14–19.

(75)   Zhang, P.; Guo, Y.-N.; Tang, J. *Coord. Chem. Rev.* **2013**, *257* (11–12), 1728–
        1763.

(76)   Jiang, W. Applications of a Configuration-Driven Unitary Group Approach to
        Electronic Structure Theory, University of North Dakota, Grand Forks, ND, 2009.

(77)   Tamukong, P. K.; Hoffmann, M. R.; Li, Z.; Liu, W. *J. Phys. Chem. A* **2014**, *118*
        (8), 1489–1501.

(78)   Li, Z.; Xiao, Y.; Liu, W. *J. Chem. Phys.* **2012**, *137* (15), 154114.

(79)   Sun, Q.; Liu, W.; Kutzelnigg, W. *Theor. Chem. Acc.* **2011**, *129* (3–5), 423–436.

(80)   Reiher, M.; Wolf, A. *J. Chem. Phys.* **2004**, *121* (22), 10945.

(81)   Mastalerz, R. P. Methodological Advances in Relativistic Quantum Chemistry,
        ETH Zurich, 2009.

(82)   Hoffmann, M. R. *J. Phys. Chem.* **1996**, *100* (15), 6125–6130.

(83)   Khait, Y. G.; Song, J.; Hoffmann, M. R. *J. Chem. Phys.* **2002**, *117* (9), 4133–4145.

(84)   Jiang, W.; Khait, Y. G.; Hoffmann, M. R. *J. Phys. Chem. A* **2009**, *113* (16), 4374–
        4380.

(85)   Khait, Y. G.; Song, J.; Hoffmann, M. R. *Int. J. Quantum Chem.* **2004**, *99* (4), 210–
        220.

(86)   Visscher, L. *Chem. Phys. Lett.* **1996**, *253* (1–2), 20–26.

(87)   Sjøvoll, M.; Gropen, O.; Olsen, J. *Theor. Chem. Accounts Theory, Comput. Model.*

(Theoretica Chim. Acta) **1997**, *97* (1–4), 301–312.

(88) Kramers, H. A. *Proc. Amsterdam Acad.* **1930**, *33*, 959–972.

(89) King, H. F.; Furlani, T. R. *J. Comput. Chem.* **1988**, *9* (7), 771–778.

(90) Harter, W. G.; Patterson, C. W. *Phys. Rev. A* **1976**, *13* (3), 1067–1082.

(91) Winter, M. Gadolinium: properties of free atoms
https://www.webelements.com/gadolinium/atoms.html (accessed Sep 3, 2017).

(92) Chen, X.; Fang, L.; Shen, X.; Lombardi, J. R. *J. Chem. Phys.* **2000**, *112* (22),
9780–9782.

(93) Connor, J. A. *Metal Clusters in Catalysis, Studies in Surface Science and
Catalysis*; Elsevier: Amsterdam, 1986.

(94) Schuh, T.; Miyamachi, T.; Gerstl, S.; Geilhufe, M.; Hoffmann, M.; Ostanin, S.;
Hergert, W.; Ernst, A.; Wulfhekel, W. *Nano Lett.* **2012**, *12* (9), 4805–4809.

(95) Chang, L.-X.; Xiong, G.; Wang, L.; Cheng, P.; Zhao, B. *Chem. Commun.* **2013**, *49*
(11), 1055–1057.

(96) Mereacre, V. M.; Ako, A. M.; Clérac, R.; Wernsdorfer, W.; Filoti, G.; Bartolomé,
J.; Anson, C. E.; Powell, A. K. *J. Am. Chem. Soc.* **2007**, *129* (30), 9248–9249.

(97) Deb, A.; Boron, T. T.; Itou, M.; Sakurai, Y.; Mallah, T.; Pecoraro, V. L.; Penner-
Hahn, J. E. *J. Am. Chem. Soc.* **2014**, *136* (13), 4889–4892.

(98) Winter, M. Dysprosium: properties of free atoms
https://www.webelements.com/dysprosium/atoms.html (accessed Sep 3, 2017).

(99)   Tang, J.; Hewitt, I.; Madhu, N. T.; Chastanet, G.; Wernsdorfer, W.; Anson, C. E.; Benelli, C.; Sessoli, R.; Powell, A. K. *Angew. Chemie Int. Ed.* **2006**, *45* (11), 1729–1733.

(100) Ren, M.; Bao, S.-S.; Hoshino, N.; Akutagawa, T.; Wang, B.; Ding, Y.-C.; Wei, S.; Zheng, L.-M. *Chem. - A Eur. J.* **2013**, *19* (29), 9619–9628.

(101) Bag, P.; Rastogi, C. K.; Biswas, S.; Sivakumar, S.; Mereacre, V.; Chandrasekhar, V. *Dalt. Trans.* **2015**, *44* (9), 4328–4340.

(102) Guo, Y.-N.; Xu, G.-F.; Gamez, P.; Zhao, L.; Lin, S.-Y.; Deng, R.; Tang, J.; Zhang, H.-J. *J. Am. Chem. Soc.* **2010**, *132* (25), 8538–8539.

(103) Ke, H.; Xu, G.-F.; Guo, Y.-N.; Gamez, P.; Beavers, C. M.; Teat, S. J.; Tang, J. *Chem. Commun.* **2010**, *46* (33), 6057.

(104) Ruiz, J.; Mota, A. J.; Rodríguez-Diéguez, A.; Titos, S.; Herrera, J. M.; Ruiz, E.; Cremades, E.; Costes, J. P.; Colacio, E. *Chem. Commun.* **2012**, *48* (64), 7916.

(105) Xue, S.; Guo, Y.-N.; Ungur, L.; Tang, J.; Chibotaru, L. F. *Chem. - A Eur. J.* **2015**, *21* (40), 14099–14106.

(106) Guo, F.-S.; Day, B. M.; Chen, Y.-C.; Tong, M.-L.; Mansikkamäki, A.; Layfield, R. A. *Angew. Chemie Int. Ed.* **2017**, *56* (38), 11445–11449.

(107) Roos, B. O.; Lindh, R.; Malmqvist, P.-Å.; Veryazov, V.; Widmark, P.-O.; Borin, A. C. *J. Phys. Chem. A* **2008**, *112* (45), 11431–11435.

(108) Kokoszka, G. F.; Padula, F.; Goldstein, A. S.; Venturini, E. L.; Azevedo, L.;

Siedle, A. R. *Inorg. Chem.* **1988**, *27* (1), 59–62.

(109) Woodward, J. R.; Cobb, S. H.; Gole, J. L. *J. Phys. Chem.* **1988**, *92* (6), 1404–1406.

(110) Hauser, A. W.; Callegari, C.; Soldán, P.; Ernst, W. E. *Chem. Phys.* **2010**, *375* (1), 73–84.

(111) Ervin, K. M.; Ho, J.; Lineberger, W. C. *J. Chem. Phys.* **1988**, *89* (8), 4514–4521.

(112) Wang, H.; Carter, E. A. *J. Phys. Chem.* **1992**, *96* (3), 1197–1204.

(113) Malcolm, N. O. J.; McDouall, J. J. W. *Mol. Phys.* **1997**, *91* (5), 917–922.

(114) Green, S. M. E.; Alex, S.; Fleischer, N. L.; Millam, E. L.; Marcy, T. P.; Leopold, D. G. *J. Chem. Phys.* **2001**, *114* (6), 2653–2668.

(115) Klotzbücher, W. E.; Petrukhina, M. A.; Nemukhin, A. V.; Ermilov, A. Y.; Grigorenko, B. L. *Spectrochim. Acta Part A Mol. Biomol. Spectrosc.* **2001**, *57* (5), 1093–1101.

(116) Fang, L.; Davis, B.; Lu, H.; Lombardi, J. R. *J. Phys. Chem. A* **2001**, *105* (41), 9375–9378.

(117) Wu, Z. J.; Zhang, H. J.; Meng, J.; Dai, Z. W.; Han, B.; Jin, P. C. *J. Chem. Phys.* **2004**, *121* (10), 4699–4704.

(118) Papas, B. N.; Schaefer, H. F. *J. Chem. Phys.* **2005**, *123* (7), 074321.

(119) Winter, M. Scandium: properties of free atoms https://www.webelements.com/scandium/atoms.html (accessed Sep 9, 2017).

(120) Kalemos, A.; Kaplan, I. G.; Mavridis, A. *J. Chem. Phys.* **2010**, *132* (2), 024309.

(121) Gazza, C. J.; Trumper, A. E.; Ceccatto, H. A. *J. Phys. Condens. Matter* **1994**, *6* (41), L625–L630.

(122) Greedan, J. E. *J. Mater. Chem.* **2001**, *11* (1), 37–53.

(123) Cano-Cortés, L.; Ralko, A.; Février, C.; Merino, J.; Fratini, S. *Phys. Rev. B* **2011**, *84* (15), 155115.

(124) Lee, S.; Jeong, J.-S.; Hwang, K.; Kim, Y. B. *Phys. Rev. B* **2014**, *90* (13), 134425.

(125) Katukuri, V. M.; Nishimoto, S.; Rousochatzakis, I.; Stoll, H.; van den Brink, J.; Hozoi, L. *Sci. Rep.* **2015**, *5* (1), 14718.

(126) Chakravarty, C.; Mandal, B.; Sarkar, P. *J. Phys. Chem. C* **2016**, *120* (49), 28307–28319.

(127) Nocera, D. G.; Bartlett, B. M.; Grohol, D.; Papoutsakis, D.; Shores, M. P. *Chem. - A Eur. J.* **2004**, *10* (16), 3850–3859.

(128) He, Z.; Kyômen, T.; Itoh, M. *Phys. Rev. B* **2004**, *70* (13), 134431.

(129) Pati, S. K.; Rao, C. N. R. *J. Chem. Phys.* **2005**, *123* (23), 234703.

(130) Nagano, A.; Naka, M.; Nasu, J.; Ishihara, S. *Phys. Rev. Lett.* **2007**, *99* (21), 217202.

(131) Bellido, N.; Simon, C.; Maignan, A. *Phys. Rev. B* **2008**, *77* (5), 054430.

(132) Naka, M.; Nagano, A.; Ishihara, S. *Phys. Rev. B* **2008**, *77* (22), 224441.

(133) Krüger, F.; Kumar, S.; Zaanen, J.; van den Brink, J. *Phys. Rev. B* **2009**, *79* (5), 054504.

(134) Lacroix, C. *Phys. B Condens. Matter* **2009**, *404* (19), 3038–3041.

(135) Knight, L. B.; Woodward, R. W.; Van Zee, R. J.; Weltner, W. *J. Chem. Phys.* **1983**, *79* (12), 5820–5827.

(136) Moskovits, M.; DiLella, D. P.; Limm, W. *J. Chem. Phys.* **1984**, *80* (2), 626–633.

(137) Walch, S. P.; Bauschlicher, C. W. *J. Chem. Phys.* **1985**, *83* (11), 5735–5742.

(138) Pápai, I.; Castro, M. *Chem. Phys. Lett.* **1997**, *267* (5–6), 551–556.

(139) Bérces, A. *Spectrochim. Acta Part A Mol. Biomol. Spectrosc.* **1997**, *53* (8), 1257–1272.

(140) Tamukong, P. K.; Theis, D.; Khait, Y. G.; Hoffmann, M. R. *J. Phys. Chem. A* **2012**, *116* (18), 4590–4601.